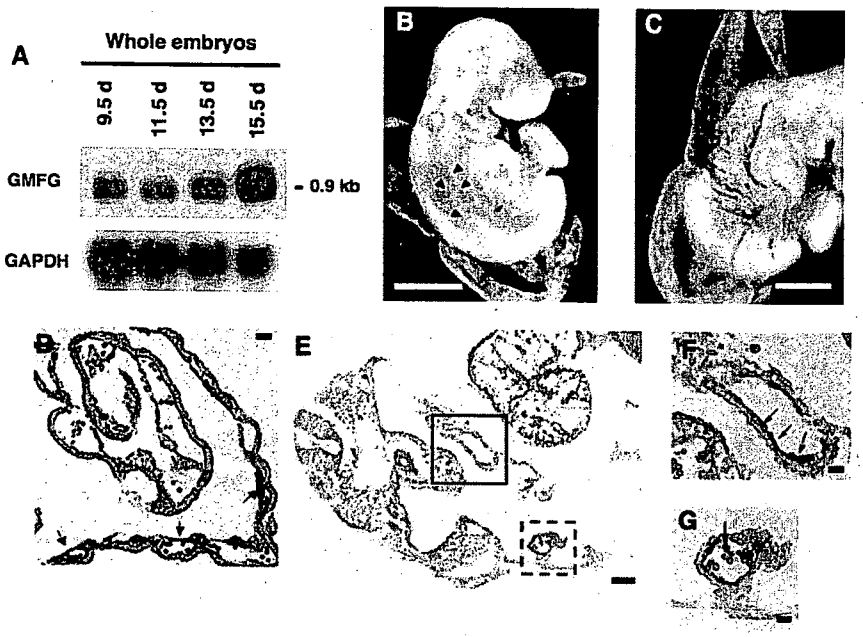

Figure 2. GMFG expression during mouse embryogenesis. A, Northern blot analysis of GMFG in whole embryos of e9.5, e11.5, e13.5, and e15.5. B, Whole-mount in situ hybridization of GMFG in e9.5d embryo. GMFG was expressed in dorsal aorta and intersomitic artery as indicated by arrowheads. C, GMFG was expressed predominantly in the yolk sac and demonstrated a spotty staining pattern. D, E, F, and G, Sections of embryo from the whole-mount in situ hybridization. GMFG expression was observed in blood islands of the yolk sac as indicated by arrows (D). GMFG was also expressed in endothelial cells and hematopoietic cells in the body (E through G). High-power views of the boxed area in E, with the solid line (F) and the broken line (G), are shown. Arrows indicate endothelial cells in F and hematopoietic cells in G. Bars are 500 μm (B and C), 100 μm (D and E), and 20 μm (F and G).

for the unique GMFG expression in microvascular endothelial cells and hematopoietic lineage-derived cells in adults.

GMFG Has a Similar Structure to Cofilin and Is Associated With F-Actin

The amino acid sequence of GMFG demonstrated significant similarity to cofilin, a key regulator of actin cytoskeleton reorganization (Figure 3A). Cofilin plays critical roles in actin dynamics through its actin-severing and actin-depolymerizing activities. Therefore, we determined to analyze GMFG function in actin cytoskeleton reorganization. We first examined the subcellular localization of GMFG and cofilin in bovine aortic endothelial cells (BAECs). Recombinant cofilin and GMFG localized preferentially in the F-actin–rich structures in membrane ruffles as well as in nucleus (Figure 3B). Furthermore, native GMFG in human microvascular endothelial cells also demonstrated colocalization with F-actin in membrane ruffles (Figure 3C). These results suggest that GMFG may play a role in actin dynamics at the leading edge of cells. We then examined if GMFG is associated with F-actin using actin co-sedimentation assay. Cell lysates from GMFG or cofilin-expressing BAECs were incubated with F-actin followed by ultracentrifugation to precipitate F-actin. Significant co-sedimentation of GMFG in the pellet was detected by immunoblotting as well as of cofilin, indicating that GMFG is associated with F-actin (Figure 3D).

GMFG Is a Phosphoprotein, and Its Phosphorylation Is Enhanced by Coexpression of Dominant Active Rac and Cdc42

Because cofilin function is tightly regulated by phosphorylation of a single N-terminal serine residue, and GMFG also has N-terminal serines at the second (Ser2) and fourth (Ser4) position (Figure 3A), we explored their possible phosphorylation in GMFG. Expression constructs of wild-type GMFG (GMFG-WT) and GMFG mutants, in which Ser2 and/or Ser4 were replaced with alanine, were transfected into BAECs. Metabolic labeling of BAECs with P^{32}-phosphate revealed that GMFG was phosphorylated in cells, and replacing Ser2 and/or Ser4 with alanine completely abolished phosphorylation (Figure 4A). These results indicate that Ser2 and/or Ser4 are the phosphorylation sites and that both Ser2 and Ser4 are essential for GMFG phosphorylation. Of note, when incubated in serum-free media, phosphorylation of GMFG significantly diminished, suggesting that phosphorylation might be enhanced by soluble factors such as growth factors (Figure 4B).

Because small GTPases play central roles in actin cytoskeleton reorganization, we investigated the effect of small GTPases on GMFG phosphorylation. Coexpression of dominant active Rac1 and Cdc42 significantly enhanced GMFG phosphorylation, whereas dominant active RhoA did not (Figure 4C). These results suggest that GMFG function might be modified by Rac and Cdc42.

GMFG Association With F-Actin Is Regulated by Phosphorylation of N-Terminal Serine

To explore the effect of phosphorylation on GMFG function, we prepared a series of GMFG mutant expression constructs in which Ser2 and/or Ser4 were replaced with alanine (SA) (nonphosphorylated mutant) or glutamic acid (SE) (pseudophosphorylated mutant). Cell lysates of BAECs expressing GMFG-WT or GMFG mutants were incubated with F-actin, and their co-sedimentation with F-actin was detected by immunoblotting. When incubated in the absence of F-actin, only minimal sedimentation was observed except in the cases of GMFG-S2/4A and GMFG-S2A where sedimentation of some insoluble fractions in the absence of F-actin were consistently observed in 3 independent experiments (Figure 4). We subtracted the background sedimentation (in the absence of F-actin) from the co-sedimentation with F-actin and regarded it as the sedimentation associated with F-actin. Interestingly, GMFG-S2/4E and especially GMFG-S2E dem-

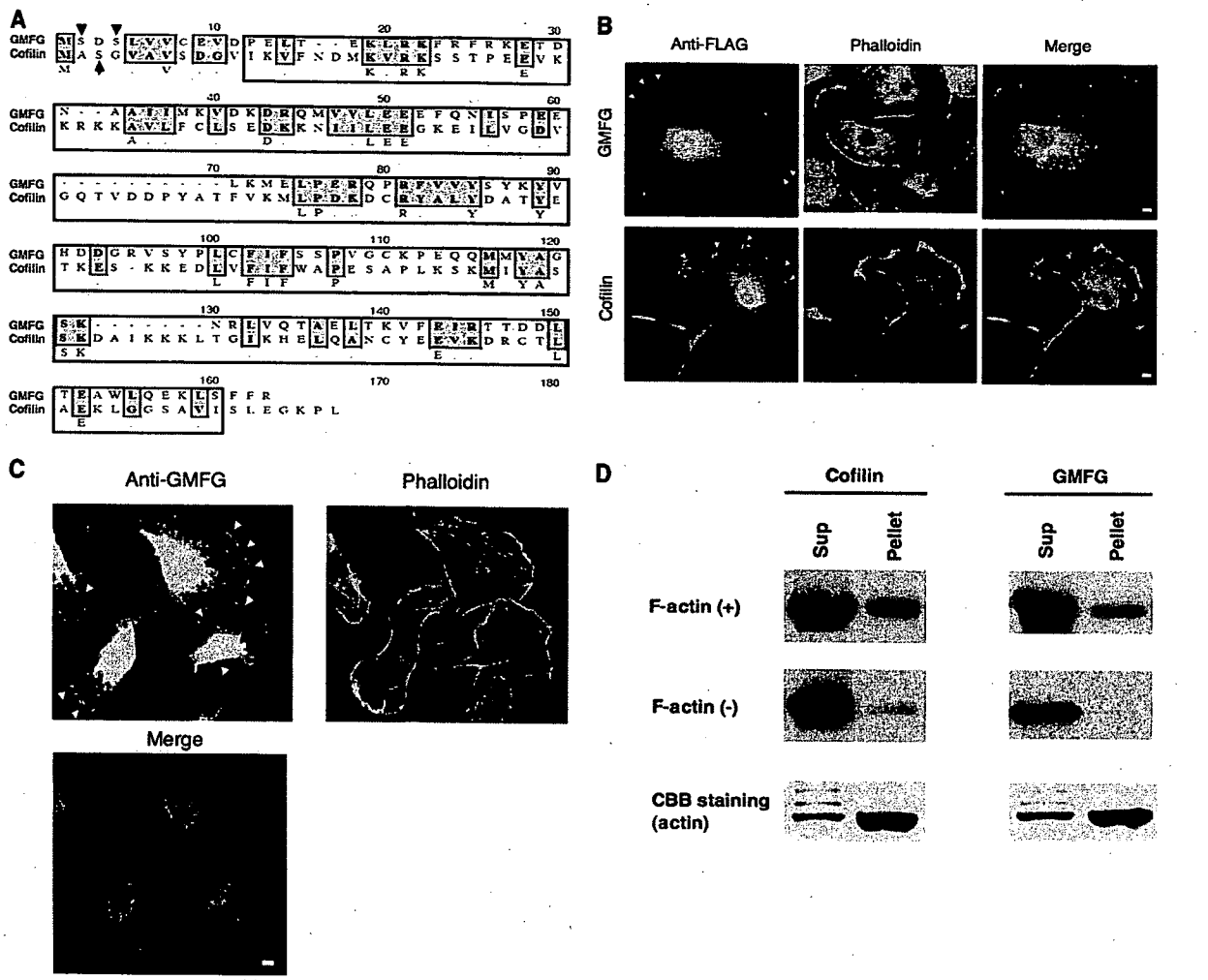

Figure 3. GMFG has a similar structure to colilin and is associated with F-actin. A, GMFG demonstrates 39% similarity to cofilin and has a similar actin-depolymerizing factor homology domain to cofilin as surrounded by a solid line. Similar amino acids between GMFG and cofilin are highlighted. Cofilin function is tightly regulated by phosphorylation of the N-terminal serine indicated by the arrow. GMFG has serines at second and fourth position as indicated by arrowheads. B, Immunostaining of F-actin and FLAG-tagged recombinant GMFG or cofilin in bovine aortic endothelial cells (BAECs). Significant localization in the forward periphery F-actin–rich structures was observed in both GMFG and cofilin as indicated by arrowheads. C, Immunostaining of F-actin and native GMFG in HMVEC. Significant localization of GMFG in the forward periphery F-actin–rich structures was observed as indicated by arrowheads. Bars=10 μm. D, Cell lysate from BAECs expressing cofilin or GMFG was incubated with F-actin followed by ultracentrifugation. Supernatants (S) and resuspended pellets (P) were run on SDS-PAGE, and the proteins of interest were detected by immunoblotting. F-actin was successfully precipitated in pellets visualized by Coomassie brilliant blue (CBB) staining. Similar results were obtained by 2 independent experiments.

onstrated significantly higher association with F-actin than other GMFG mutants or GMFG-WT, suggesting that phosphorylation of Ser2 but not Ser4 enhances GMFG association with F-actin. To exclude the possibility that replacement of N-terminal serine with alanine caused inappropriate protein folding or localization, we examined the subcellular localization of recombinant GMFG-S2/4A, GMFG-S2A, and GMFG-S4A. They demonstrated similar subcellular localization to GMFG-WT, suggesting that replacement of N-terminal serine with alanine did not cause inappropriate protein folding or localization (Figure 5B).We also confirmed that recombinant GMFG mutant of which serine(s) was replaced with glutamic acid(s) demonstrated proper subcellular localization (data not shown). It is intriguing that although the affinity of GMFG and cofilin for F-actin is regulated by phosphorylation of the N-terminal serine, phosphorylation enhances GMFG binding, whereas it reduces cofilin binding to F-actin.

GMFG Is a Novel Factor in Actin Cytoskeleton Reorganization

Because cofilin directly affects actin filament turnover, we investigated the effects of GMFG on actin cytoskeleton reorganization. Somewhat surprisingly, HeLa cells transiently transfected with GMFG-WT or the pseudophosphorylated form of GMFG (GMFG-S2E) demonstrated no significant change in F-actin structure, whereas expression of wild-type cofilin (cofilin-WT) or the active form of cofilin (cofilin-S3A) significantly reduced F-actin structure (Figure 6A). These results suggest that GMFG does not have a significant actin-depolymerizing activity and may have a different function in actin dynamics from cofilin.

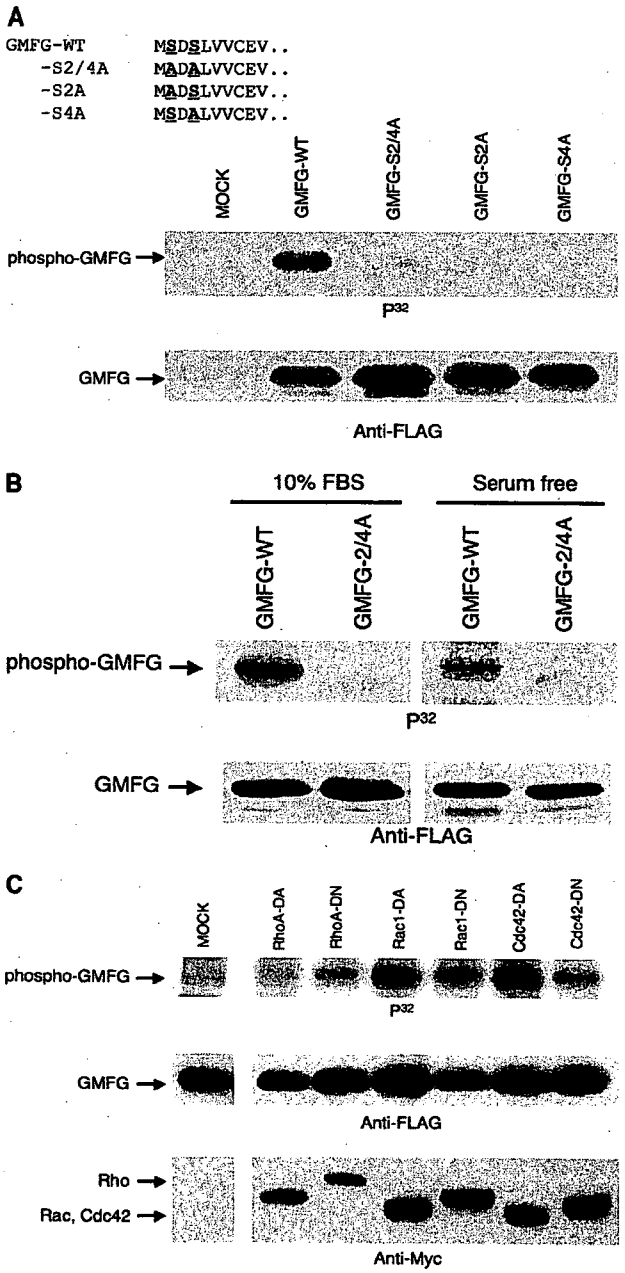

Figure 4. GMFG is a phosphoprotein. A, BAECs expressing the wild-type GMFG (GMFG-WT), GMFG mutants, or empty vector (MOCK) were labeled with P^{32}-phosphate. Immunoprecipitated GMFG was run on SDS-PAGE and the phosphorylated GMFG was visualized by autoradiography. Whole GMFG expression was detected by immunoblotting using anti-FLAG M2 antibody. Results were confirmed by 3 independent experiments. B, BAECs expressing GMFG were incubated either in growth media or serum-free media for overnight followed by labeling with P^{32}-phosphate. C, GMFG was coexpressed with either dominant active (DA) or dominant negative (DN) form of Rho, Rac, and Cdc42 or empty vector (MOCK). Cells were labeled with P^{32}-phosphate, and GMFG phosphorylation was visualized by autoradiography. GMFG and small GTPase expressions were detected by immunoblotting using anti-FLAG M2 and anti-myc 9E10 antibody, respectively. Similar results were obtained by 3 independent experiments.

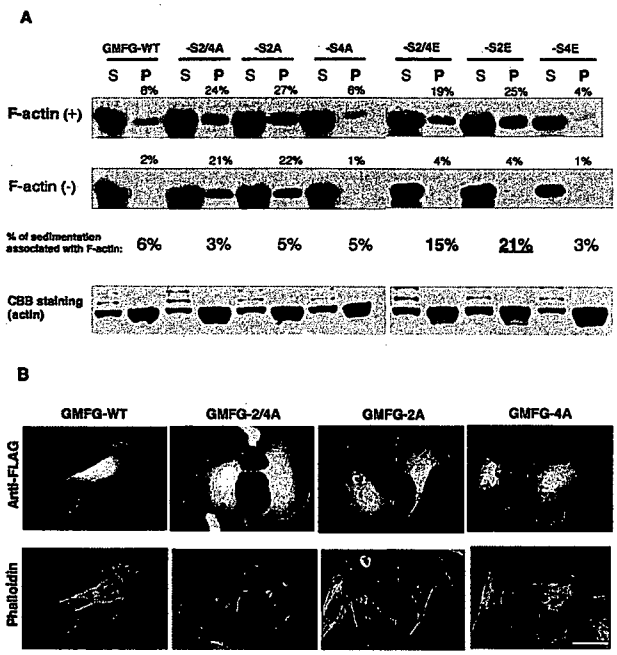

Figure 5. GMFG is associated with F-actin. A, Actin co-sedimentation assay was performed as described in Figure 2D. Pseudophosphorylation of Ser2 significantly enhanced GMFG association with F-actin. Similar results were obtained by 3 independent experiments. B, Immunostaining of recombinant GMFG-WT or GMFG mutants and F-actin in BAECs. Bar=50 μm.

We then generated HeLa cells stably expressing cofilin-WT, cofilin-S3A, GMFG-WT, GMFG-S2E, and GMFG-S4E. Because HeLa cells are the most widely used and the most-characterized cells for the research of actin cytoskeleton reorganization, we chose HeLa cells to analyze GMFG function in actin cytoskeleton reorganization. Stable expression of transgenes and recombinant proteins were confirmed by RT-PCR and immunoblotting respectively (data not shown). Large populations (≈30%) of cells stably expressing cofilin-S3A (HeLa/cofilin-S3A) demonstrated enhanced membrane ruffles formation under the basal culture condition, whereas none of the other stable transfectants demonstrated such a phenotype (Figure 6B and 6C).

On the other hand, when cells were stimulated with a low concentration (100 ng/mL) of EGF following the incubation in serum-free media for 24 hours, HeLa/GMFG-S2E demonstrated significant stimulus-responsive lamellipodia and subsequent ruffles formation (Figure 6D and 6E). HeLa/GMFG-WT also demonstrated less but significant stimulus-responsive lamellipodia formation with 100 ng/mL EGF treatment (Figure 6D and 6E). None of the other transfectants, including HeLa/MOCK, demonstrated such an effect. Stimulation with 1000 ng/mL EGF induced stimulus-responsive lamellipodia and subsequent ruffle formation in all stable transfectants (data not shown). These results suggest a significant role of GMFG in stimulus-responsive actin polymerization. Despite its structural similarity, GMFG appears to play a different role from cofilin in actin cytoskeleton reorganization. It has been reported that twinfilin, another actin-depolymerizing factor domain family protein, does not have actin-depolymerizing activity and functions in actin dynamics in clearly distinct manner from cofilin.[8] Moreover,

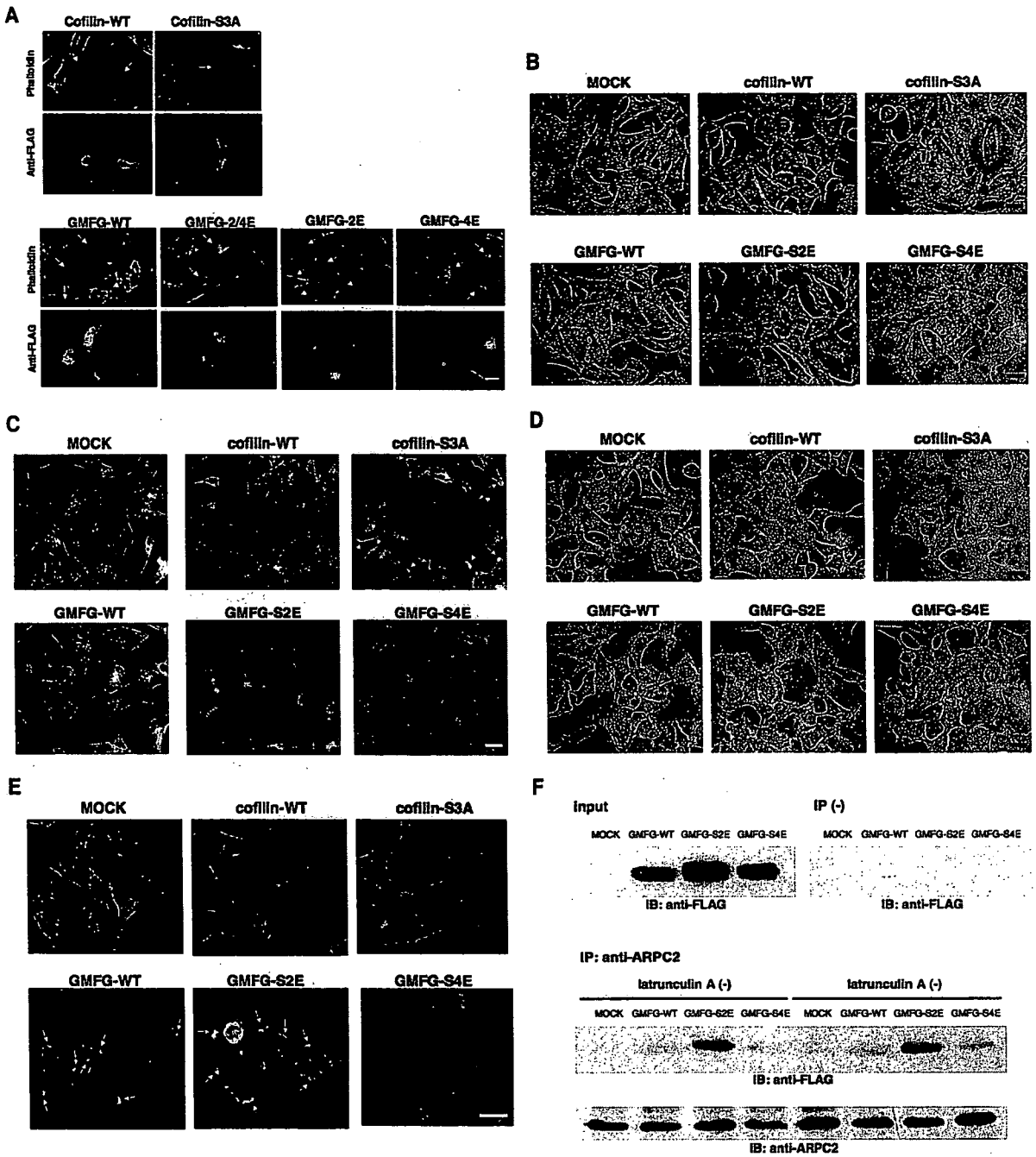

Figure 6. GMFG enhances stimulus-responsive lamellipodia formation, presumably through its interaction with Arp2/3 complex. A, F-actin and recombinant protein were visualized in HeLa cells expressing the protein of interest. Arrows indicate cells expressing the designated protein. B, Images of HeLa cells stably expressing the protein of interest under the basal culture condition by the phase-contrast microscopy. C, F-actin were visualized in HeLa cells under the same condition as in B. Arrows indicate the enhanced membrane ruffles formation. D, HeLa cells stably expressing the protein of interest were incubated in serum-free media for 24 hours, followed by stimulation with 100 ng/mL EGF. Stimulus-responsive lamellipodia and subsequent membrane ruffles formation are indicated by arrows. E, F-actin were visualized in HeLa cells under the same condition as in D. Arrows indicate the stimulus-responsive lamellipodia and subsequent membrane ruffles formation. Bars=40 μm. Similar results were obtained by 2 independent experiments. F, Arp2/3 complex in the cell lysate was immunoprecipitated with anti-ARPC2 antibody. Coprecipitation of GMFG with Arp2/3 complex was detected by immunoblotting. To exclude the potential nonspecific interactions from coprecipitation of actin filaments, 40 μmol/L latrunculin A was included in the immunoprecipitation reactions. Results were confirmed by 2 independent experiments.

Abp1p, an actin binding protein originally isolated from yeast, also has an actin-depolymerizing factor homology domain, but it binds to Arp2/3 complex and activates the actin nucleation, not actin depolymerization.[13]

To better understand the cellular mechanisms by which GMFG enhances stimulus-responsive lamellipodia formation, we investigated the possible interaction of GMFG with the Arp2/3 complex, a key regulator of stimulus-responsive actin

polymerization. Cell lysates expressing GMFG were incubated with anti–Arp2/3 complex subunit 2 (ARPC2) antibody, and coprecipitation of GMFG with ARPC2 was detected by immunoblotting. To exclude the potential nonspecific interactions from coprecipitation of actin filaments, 40 μmol/L latrunculin A was included in the immunoprecipitation reactions. Immunoblotting confirmed no detectable actin in the pellets (data not shown). GMFG was coprecipitated with ARPC2, suggesting GMFG interaction with Arp2/3 complex (Figure 6F). Of note, more GMFG-S2E was pulled down than GMFG-WT or GMFG-S4E, indicating that phosphorylation of Ser2 enhances GMFG interaction with the Arp2/3 complex (Figure 6F). These results suggest that in response to extracellular stimuli, GMFG might be phosphorylated at Ser2 through Rac and Cdc42, promoting its interaction with Arp2/3 complex as well as with F-actin, which then accelerates stimulus-responsive actin polymerization at the leading edge of cells. However, further analysis is certainly required to conclude its functional relevance with Rac and Cdc42. Given that even pseudophosphorylated form of GMFG required exogenous stimulus to modulate actin cytoskeleton reorganization, GMFG binding to Arp2/3 complex is not sufficient to initiate new actin polymerization.

GMFG Positively Regulates Actin-Based Cellular Functions

We then investigated GMFG functions in actin-based cellular functions in endothelial cells. As shown in Figure 1B, BAECs express only a minimal amount of GMFG, much less than in microvascular endothelial cells. Therefore, we used BAECs to examine the effect of GMFG overexpression on actin-based cellular functions. The majority of cells expressed the transgene 24 hours after transfection, as assessed by GFP-construct transfection (supplemental Figure II). BAECs overexpressing GMFG demonstrated significantly higher motility than mock-transfected BAECs (Figure 7A). Moreover, BAECs overexpressing GMFG demonstrated significantly enhanced tube formation on Matrigel as compared with the mock-transfected cells (Figure 7B). These results suggest that GMFG positively regulates actin-based cellular functions in endothelial cells, presumably through accelerating stimulus-responsive actin polymerization.

Finally, we examined GMFG expression in a cardiac ischemia/reperfusion model because both angiogenesis and inflammation play important roles in the pathophysiology of ischemic cardiovascular diseases. GMFG expression was significantly increased in the ischemia/reperfusion tissues (Figure 7C and 7D). Although further analysis, such as immunohistochemistry to clarify the cells express GMFG, is certainly needed to address GMFG function in the ischemia/reperfusion heart, this result suggests possible GMFG involvement in the pathophysiology of cardiovascular diseases.

Our data define a novel pathway in the regulation of actin cytoskeleton reorganization and actin-based cellular functions (Figure 7E). Given that inflammatory cells and endothelial cells have a close relationship and interact with each other in ischemic cardiovascular diseases, GMFG may play a role in the pathophysiology of such diseases.[14,15]

Discussion

GMFG is preferentially expressed in human microvascular endothelial cells but not in endothelial cells from other vascular beds. Given that microvascular endothelial cells are the most important cellular players in angiogenesis in adults and expression of GMFG enhanced migration and tube formation in BAECs, GMFG may play a role in angiogenesis in adults. During embryogenesis, GMFG is predominantly expressed in blood islands of the yolk sac, in which hematopoietic and endothelial lineages develop simultaneously in close proximity, suggesting GMFG functions in embryonic vasculogenesis as well as hematopoiesis. This may also well correlate with the unique GMFG expression in microvascular endothelial cells and inflammatory cells seen in adults. In support of this contention, a search of the database of microarray analysis at the National Center for Biotechnology Information revealed that GMFG is expressed in a variety of hematopoietic cells such as T cell, B cell, NK cell, monocyte, and dendritic cell, as well as hematopoietic progenitor cells including $CD34^+$ and $CD105^+$ bone marrow cells, which may give rise to endothelial progenitor cells.[16,17]

Our findings demonstrated that GMFG plays a significant role in actin cytoskeleton reorganization distinct from cofilin, despite structural similarity. Stable expression of the pseudophosphorylated form of GMFG remarkably enhanced stimulus-responsive lamellipodia and subsequent membrane ruffles formation, presumably through interaction with Arp2/3 complex. In response to extracellular stimuli, active Rac and Cdc42 might activate GMFG via phosphorylation of Ser2 as well as WASP/WAVE. Binding of phosphorylated GMFG to the Arp2/3 complex might accelerate stimulus-responsive actin polymerization cooperating with active WASP/WAVE, resulting in enhanced actin-based cellular functions. However, further analysis is required to verify this hypothesis.

Of note, the pseudophosphorylated form of GMFG did not affect actin cytoskeleton reorganization in HeLa cells under basal culture conditions, although it remarkably enhanced stimulus-responsive lamellipodia formation. These results suggest that binding of GMFG to Arp2/3 complex is not sufficient to initiate new actin polymerization, but once Arp2/3 complex is activated by other activator such as WASP/WAVE, GMFG may enhance Arp2/3 complex-induced actin polymerization. Therefore, GMFG may enhance actin-based cellular functions only in the presence, and under the control, of endogenous stimulators such as growth factors and cytokines. In this regard, GMFG may be a good target for gene therapy because unexpected adverse effect caused by dysregulated transgene function is a considerable concern for the clinical application of gene therapy.

Our results indicate that GMFG is a novel factor in actin cytoskeleton reorganization and that it modulates actin-based cellular function in microvascular endothelial cells, inflammatory cells, and possibly hematopoietic progenitor cells. Because these cells are essential players in angiogenesis, vasculogenesis, and immune system function, and each of them plays specific roles in ischemic cardiovascular diseases, we believe that further analysis of GMFG will provide new insights into the molecular mechanisms of these diseases and

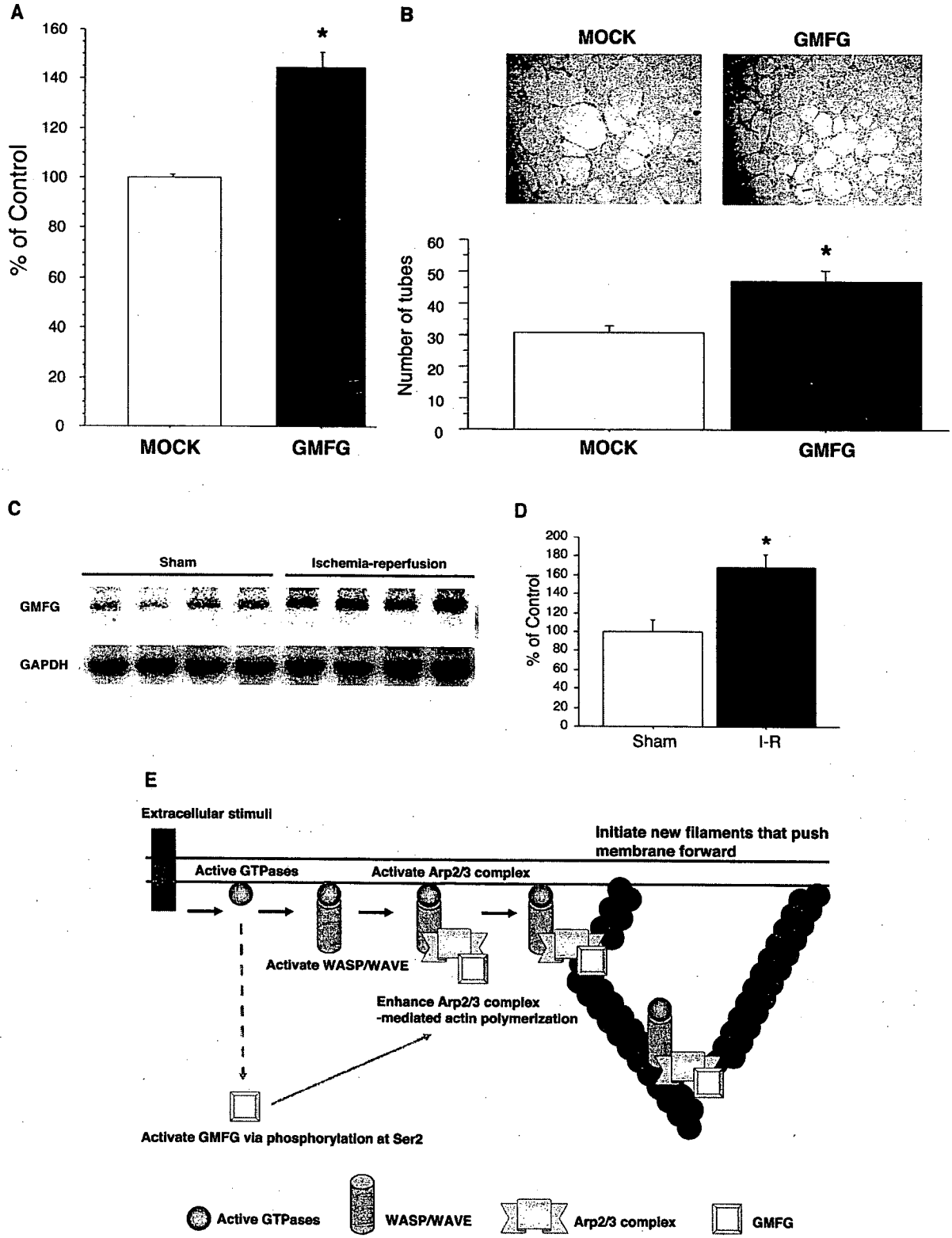

Figure 7. GMFG enhances actin-based cellular functions in endothelial cells. A, Cell motility of BAECs transiently transfected with GMFG or empty vector was examined by modified Boyden chamber assay (n=3). BAECs expressing GMFG demonstrated more motility than mock-transfected cells (*$P<0.0001$ vs MOCK). B, BAECs transfected with GMFG or empty vector were plated on Matrigel and incubated for 60 hours. Their tube-formation capacity was quantified by the number of tubes counted in 5 independent fields. BAECs expressing GMFG demonstrated significantly enhanced tube-formation capacity than mock-transfected cells (*$P<0.005$ vs MOCK) (n=2). C, Northern blot analysis of GMFG in the left ventricles from sham-operated (sham) or ischemia/reperfusion (I-R) model mice. D, Quantitative analysis of GMFG expression corrected by GAPDH. GMFG expression in ischemia/reperfusion left ventricles was significantly higher than in sham control (*$P<0.02$ vs sham control). E, Schematic diagram of GMFG pathway in actin dynamics.

that GMFG may be an attractive new target for pharmacotherapeutic agents to treat such diseases.

Acknowledgments

We thank Dr Kiyofumi Asai for providing the anti-sera for GMFG. We thank Dr Yoshimi Takai for providing the expression constructs of dominant active and dominant negative Rho, Rac, and Cdc42. We thank Dr Alex Dunn for helpful suggestions for actin-binding and Arp2/3 complex–binding assays.

Source of Funding

This work was supported by the Donald W. Reynolds Foundation.

Disclosures

None.

References

1. Ho M, Yang E, Matcuk G, Deng D, Sampas N, Tsalenko A, Tabibiazar R, Zhang Y, Chen M, Talbi S, Ho YD, Wang J, Tsao PS, Ben-Dor A, Yakhini Z, Bruhn L, Quertermous T. Identification of endothelial cell genes by combined database mining and microarray analysis. *Physiol Genomics*. 2003;13:249–262.
2. Asai K, Fujita K, Yamamoto M, Hotta T, Moriyama M, Kokubo M, Moriyama A, Kato T. Isolation od novel cDNA (hGMF-gamma) homologous to glia maturation factor-beta gene. *Biochim Biophys Acta*. 1998;1396:242–244.
3. Pollard TD, Blanchoin L, Mullins RD. Molecular mechanisms controlling actin filament dynamics in nonmuscle cells. *Annu Rev Biophys Biomol Struct*. 2000;29:545–576.
4. Carlier MF, Ressad F, Pantaloni D. Control of actin dynamics in cell motility. Role of ADF/cofilin. *J Biol Chem*. 1999;274:33827–33830.
5. Yamazaki D, Suetsugu S, Miki H, Kataoka Y, Nishikawa S, Fujiwara T, Yoshida N, Takenawa T. WAVE2 is required for directed cell migration and cardiovascular development. *Nature*. 2003;424:452–456.
6. Bamburg JR, Wiggan OP. ADF/cofilin and actin dynamics in disease. *Trends Cell Biol*. 2002;12:598–605.
7. Zhang J, Shehabeldin A, da Cruz LA, Butler J, Somani AK, McGavin M, Kozieradzki I, dos Santos AO, Nagy A, Grinstein S, Penninger JM. Antigen receptor-induced activation and cytoskeletal rearrangement are impaired in Wiskott-Aldrich syndrome protein-deficient lymphocytes. *J Exp Med*. 1999;190:1329–1342.
8. Goode BL, Drubin DG, Lappalainen P. Regulation of the cortical actin cytoskeleton in budding yeast by twinfilin, a ubiquitous actin monomer-sequestering protein. *J Cell Biol*. 1998;142:723–733.
9. Bamburg JR. Proteins of the ADF/cofilin family: essential regulators of actin dynamics. *Annu Rev Cell Dev Biol*. 1999;15:185–230.
10. Ghosh M, Song X, Mouneimne G, Sidani M, Lawrence DS, Condeelis JS. Cofilin promotes actin polymerization and defines the direction of cell motility. *Science*. 2004;304:743–746.
11. Hirata KI, Ishida T, Penta K, Rezaee M, Yang E, Wohlgemuth J, Quertermous T. Cloning of an immunoglobulin family adhesion molecule selectively expressed by endothelial cells. *J Biol Chem*. 2001;276:16223–16231.
12. Ikeda K, Quertermous T. Molecular isolation and characterization of a soluble isoform of activated leukocyte cell adhesion molecule that modulates endothelial cell function. *J Biol Chem*. 2004;279:55315–55323.
13. Olazabal IM, Machesky LM. Abp1p and cortactin, new "hand-holds" for actin. *J Cell Biol*. 2001;154:679–682.
14. Nian M, Lee P, Khaper N, Liu P. Inflammatory cytokines and postmyocardial infarction remodeling. *Cir Res*. 2004;94:1543–1553.
15. Naldini A, Carraro F. Role of inflammatory mediators in angiogenesis. *Curr Drug Targets Inflamm Allergy*. 2005;4:3–8.
16. Asahara T, Murohara T, Sullivan A, Silver M, van der Zee R, Li T, Witzenbichler B, Schatteman G, Isner JM. Isolation of putative progenitor endothelial cells for angiogenesis. *Science*. 1997;275:964–967.
17. Salven P, Mustjoki S, Alital R, Alitalo K, Rafii S. VEGFR-3 and CD133 identify a population of CD34+ lymphatic/vascular endothelial precursor cells. *Blood*. 2003;101:168–172.

Available online at www.sciencedirect.com
SCIENCE DIRECT
Journal of Molecular and Cellular Cardiology 40 (2006) 799–809
Journal of Molecular and Cellular Cardiology
www.elsevier.com/locate/yjmcc

Original article

Myocardium-targeted delivery of endothelial progenitor cells by ultrasound-mediated microbubble destruction improves cardiac function via an angiogenic response

Kan Zen [a], Mitsuhiko Okigaki [a,*], Yohei Hosokawa [b], Yasushi Adachi [c], Yoshihisa Nozawa [d], Michitaka Takamiya [a], Tetsuya Tatsumi [a], Norifumi Urao [a], Kento Tateishi [a], Tomosaburo Takahashi [a], Hiroaki Matsubara [a]

[a] *Department of Cardiovascular Medicine, Kyoto Prefectural University of Medicine, Kamigyo-ku, Kyoto, 602-8566, Japan*
[b] *Department of Pathology, Omihachiman City Hospital, Japan*
[c] *First Department of Pathology, Kansai Medical University, Japan*
[d] *Pharmacobioregulation Research Laboratory, Taiho Pharmaceutical Co. Ltd, Saitama, Japan*

Received 24 January 2006; accepted 14 March 2006
Available online 5 May 2006

Abstract

Application of ultrasound-mediated destruction of microbubbles (US + Bubble) to skeletal muscle creates capillary ruptures leading to leakage of the cell components. We studied whether US + Bubble combined with bone-marrow-derived mononuclear cells (BM-MNCs) infusion enables the targeted delivery of endothelial-lineage cells into the myocardium and improves cardiac function of the cardiomyopathy model due to the paucity of neocapillary formation. Pulsed US was applied to the anterior chest of BIOTO2 cardiomyopathy hamsters for 90 s after the intravenous injection of microbubble (Optison^{R}) followed by infusion of BM-MNCs. Cardiac samples from US + microbubble + BM-MNCs (US + Bubble + BM), US + Bubble, US + BM without Bubble, and saline infusion control groups were analyzed 12 weeks after treatment. Labeled BM-MNCs transplanted by US + Bubble were found to be mainly localized in the microvessels, but not by US stimulation without microbubble (121.2 ± 24.5 vs. 2.80 ± 1.30 cells/mm^2, $P < 0.001$). Capillary densities in US + Bubble + BM group were increased 1.7-fold ($P < 0.05$) over the control, and neither US + Bubble nor US + BM enhanced neocapillary formation. ^{99m}Tc-Tetrofosmin scintigraphy revealed that blood perfusion area in the US + Bubble + BM group was 48% greater than the control ($P < 0.01$). US + Bubble stimulation induces the expression of adhesion molecules (VCAM-1 and ICAM-1) in capillaries, and the US + Bubble-mediated supply of BM-MNCs increased the myocardial content of VEGF and bFGF. The left ventricular wt/body wt, area of cardiac fibrosis, and apoptotic cell numbers in the US + Bubble + BM group significantly ($P < 0.05$) decreased by 82%, 73%, and 64% relative to the control, respectively. The cardiac function in myopathic hamsters (assessed by fractional shortening) was markedly improved 36% ($P < 0.05$) by US + Bubble + BM treatment. Targeted delivery of BM-MNCs by US + Bubble to the myocardium of the cardiomyopathic hamster increased the capillary densities and regional blood flow and inhibited cardiac remodeling, resulting in the prevention of heart failure. This non-invasive cell delivery system may be useful as a novel efficient approach for angiogenic cell therapy to the myocardium.

Keywords: Angiogenesis; Endothelial progenitor; Ultrasound; Microbubble; Cardiomyopathy

1. Introduction

Cardiovascular diseases are often caused by a decrease in blood perfusion. Medical interventions to restore blood supply cannot be applied to all the patients. To treat those who are not candidates for conventional revascularization, alternative salvage therapy for neovascularization needs urgently to be developed. Recently, bone-marrow-derived endothelial progenitor cells (BM-EPCs) were isolated from the mononuclear cell (MNC) population in the peripheral blood [1,2]. These cells have a high proliferative activity and differentiated into ECs [2], suggesting that they may have the potential to accelerate neovascularization in the ischemic tissue. EPCs that were expanded from the adult peripheral or the cord blood

* Corresponding author. Fax: +81 75 251 5514.
E-mail address: okigakim@koto.kpu-m.ac.jp (M. Okigaki).

0022-2828/$ - see front matter © 2006 Elsevier Inc. All rights reserved.
doi:10.1016/j.yjmcc.2006.03.012

enabled the increase in the capillary density (CD) in the ischemic hindlimb [3,4]. Based on this basic research, the intramuscular transplantation of BM-MNCs has been clinically applied to induce angiogenesis in the ischemic limb [5]. Furthermore, clinical trials of catheter-based autologous BM-MNCs delivery approaches, intracoronary transfer for acute myocardial infarction [6–9], or intramyocardial injection for ischemic cardiomyopathy [10–12] resulted in an improvement of symptoms, blood perfusion, and function.

Besides obtaining diagnostic ultrasound (US) images, contrast agent microbubbles have been currently used for therapeutic purposes. US-mediated microbubble destruction in the capillary lumen elicits arteriogenesis and enhanced the hyperemic blood flow in normal [13] and ischemic [14] rat skeletal muscle. Microbubble destruction creates pores in the capillary walls, and this effect is dependent on the applied ultrasound power [13,15–17]. This method was applied to the targeted drug and gene delivery to the arterial vasculature [18,19] and tissue [20–23]. Targeted transfer of hepatocyte growth factor gene by US–microbubble destruction to cardiomyopathic hearts leads to the prevention of myocardial injury through angiogenesis actions [24,25].

Deterioration of cardiac function in the BIOTO2 cardiomyopathic hamster is attributed to a defect in δ-sarcoglycan that disrupts the dystrophin-associated glycoprotein complex, in which myocyte loss progresses in two ways. First, numerous vessel segments with constrictions and focal luminal narrowing develop. These vessel irregularities lead to focal ischemic injury and necrosis, resulting in myocyte loss [26]. Second, myocyte loss progresses owing to Ca^{2+} overload caused by high basal activity of Ca^{2+}-permeable channels or mechanosensitive Ca^{2+}-permeable channels [27]. In fact, Shimizu et al. [28] demonstrated the decreases in capillary numbers in the BIOTO2 myocardium by the histological examination and angiography using synchrotron radiation and concluded that impaired neoangiogenesis is involved in the progression of cardiac function in the BIOTO2. Furthermore, since Taniyama et al. reported that the angiogenetic gene therapy using hepatic growth factor (HGF) effectively increases the regional blood flow and prevents the progression of heart failure in the similar cardiomyopathic hamster BIO14.6 model [24]. Based on these previous findings, we attempted to study whether the increase in the regional blood perfusion by angiogenic cell therapy can prevent the progression of myocyte injury in the BIOTO2 hamster model.

The present study demonstrates that the intravenous infusion of BM-MNCs combined with US + Bubble enabled targeted delivery of BM-MNCs to the BIOTO2 myopathic hearts and induced the regional angiogenic response, resulting in an improvement of heart failure associated with the inhibition of cardiac remodeling and myocyte apoptosis. These findings suggest that this novel targeted cell delivery approach may be feasible as a non-invasive angiogenic cell therapy to the myocardium.

2. Materials and methods

2.1. Isolation of MNCs from the bone marrow

BM-MNCs were isolated by Percoll gradient centrifugation (Nycoprep, AXIS-SHIELD, Oslo, Norway) [29]. All animal experiments were approved by the Animal Care and Use Committee of Kyoto Prefectural University.

2.2. BM-MNCs delivery into the myocardium with microbubble–US

Eight-week-old BIOTO2 hamsters (Bio Breeders, Fitchburg, MA) were irradiated with low-frequency US (1 MHz, 50% duty ratio; ITO-US-3, Ito Co. Ltd, Tokyo, Japan) at an intensity of 2.0 W/cm^2 for 90 s, along with the intravenous injection of 200 μl microbubble (Optison, Mallincklodt Inc) and 300 μl saline, including 1×10^8 BM-MNCs. To prevent allograft rejection, recipients were administrated immunosuppressant FK-506 (1 mg/kg/day; Fujisawa Pharmaceutical Co., Osaka, Japan) using a mini-osmotic pump (Alzet 2004; Alza Co, Palo Alto, CA).

2.3. Tracking donor BM-MNCs

Donor BM-MNCs were labeled with 1,1′-dioctadecyl-3,3,3′,3′-tetramethylindocarbocyanine perchlorate (DiI, Molecular Probes, Inc) and infused to the recipient animals. After the indicated periods, hearts were frozen-sectioned and incubated with anti-von Willebrand factor (vWF) antibody (Santa Cruz Biotechnology, Inc, sc-8068) followed by FITC-conjugated secondary antibody. DiI+/vWF+ double-positive fluorescent cells were evaluated.

2.4. Histological and immunohistochemical analyses

Twelve weeks after BM-MNC delivery, the frozen-sectioned hearts were stained by alkaline phosphatase (ALP) with indoxyl tetrazolium to measure viable vessel densities in randomly selected, ten microscopic fields. The paraffin-sectioned samples were also stained with Hematoxylin–Eosin or Sirius red, and the area of cardiac muscle fiber and collagen content was evaluated, respectively. Apoptotic cardiomyocytes were evaluated in frozen-sectioned samples with an In situ Cell Death detection kit (Roche) with diaminobenzidine (DAB) and counterstained with 0.5% methyl green (Sigma). For VCAM-1, ICAM-1, interleukin 1-beta (IL-1β), tumor necrosis factor-alpha (TNF-α), monocyte chemoattractant protein-1 (MCP-1), and macrophage/monocyte immunostaining, we used the rat model as their anti-hamster antibodies were not available. Two days after US + Bubble treatment to the Wistar rats, the paraffin-sectioned hearts were immunostained by anti-rat VCAM-1 (Santa Cruz Biotechnology), ICAM-1 (ENDOGEN), IL-1β (Santa Cruz Biotechnology), TNF-α (Biosource), MCP-1 (Abcam), and CD68 (ED-1, Serotec) with DAB counterstained with Hematoxylin. The frozen-sectioned hearts were also immunostained with anti-FITC-conjugated rat VCAM-1 or anti-PE-conjugated rat vWF antibodies (BD Pharmingen). Double immunostaining using anti-rat VCAM-1 (horse radish peroxidase: brown) and anti-CD68 (alkaline phosphatase: red) antibodies with DAB and naphtol, respectively, was also performed.

2.5. Immunocytochemistry

1×10^5 BM-MNCs were primarily cultured on fibronectin-coated chamber slides (Becton Dickinson) for 7 days with EBM-2 medium supplemented with 5%FBS, EGM-2-MV-SingleQuots (Clonetics), and then incubated with 2.4 μl/ml of DiI-labeled acetylated LDL (Molecular Probes) and 10 ng/ml of BS-1-FITC (Sigma). The double-stained cells were counted as EPCs.

2.6. Western blot and real-time polymerase chain reaction (PCR) analysis

At the indicated period after BM-MNCs infusion, the hamster LV lysates were subjected to Western blot analysis with antibodies against VCAM-1 and ICAM-1 (Santa Cruz Biotechnology) or antibodies against VEGF (R&D Systems) and basic FGF (Upstate), respectively, and visualized using an ECL detection kit (Amersham).

Two days after US + Bubble treatment to the Wistar rats, total RNA was extracted from LV and then the real-time PCR was performed using the commercial kit (QIAGEN). The IL-1β, TNF-α, and MCP-1 mRNA amounts in the US + Bubble-treated heart were compared with that of the non-treated group.

2.7. Monitoring cardiac blood flow with ^{99m}Tc-Tetrofosmin scintigraphy

Cardiac blood flow was evaluated with the ratio of cardiac uptaken to the total dosed radioactivity of ^{99m}Tc-Tetrofosmin. The frozen short-axis-sectioned hearts (50 μm thickness) at the mid-ventricle level were exposed to an imaging plate, and a radioactive image was obtained using a Bio Imaging Analysis System (FUJI Photo Film).

2.8. Evaluation of the ventricular dimension and function by echocardiography

Transthoracic M-mode echocardiogram (SONOS 5500; Hewlett-Packard) was obtained by the parasternal short axis at mid-papillary muscle levels, and the LV end-diastolic dimension (LVDd) and percent fractional shortening (%FS) were determined.

2.9. Statistics

Statistical analyses were performed with one-way ANOVA followed by pair-wise contrasts using Dunnett's test. Data

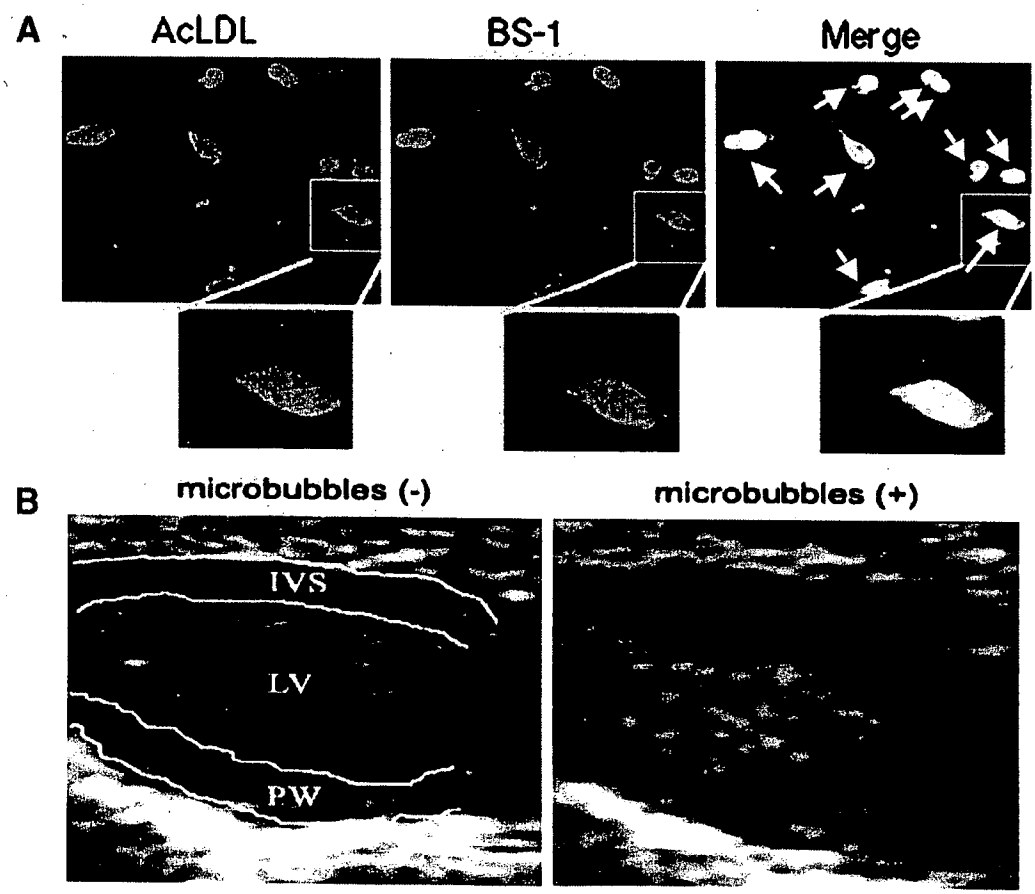

Fig. 1. EPC properties of BM-MNCs and the echocardiographic microbubble image. (A) BM-MNCs were cultured on fibronectin-coated plates for 7 days, and their binding ability to FITC-BS-1-Lectin and uptake of DiI-AcLDL was examined. BS-1+/AcLDL+ double fluorescent cells (arrows) in the merged image are considered to be the endothelial-lineage cells that exhibit a spindle shape. (B) The echocardiographical image (arrows) of microbubble delivery into the LV cavity immediately after microbubble injection. LV: left ventricle, IVS: intra-ventricular septum, PW: posterior wall. Scale bar indicates 100 μm.

(means ± SE) were considered statistically significant when P was <0.05.

3. Results

3.1. Incidence of endothelial-lineage cells in BM-MNCs

Immunocytochemical analysis indicated that 76 ± 2% of 7-day-cultured BM-MNCs (prepared from the BIOTO2 hamster) incorporated DiI-AcLDL and bound FITC-BS-1 (n = 5), some of which exhibited a spindle shape (Fig. 1A), suggesting that endothelial-lineage cells were considered to be included in this fraction as reported [5,30].

3.2. Targeted delivery of BM-MNCs to the myocardium by ultrasound-mediated microbubble destruction

US was applied to the anterior chest for 90 s immediately after intravenous injection of microbubble (Optison^R) into the BIOTO2 hamster followed by infusion of DiI-labeled 1 × 10^8 BM-MNCs. Echocardiography confirmed that microbubble was actually delivered into the LV cavity a few seconds after injection (Fig. 1B).

The transfused DiI-positive BM-MNCs were detected in the myocardium 2 weeks after US + Bubble stimulation but barely detectable by the US treatment alone without microbubble injection (121.2 ± 24.5 vs. 2.8 ± 1.3 cells/mm^2, n = 10, P < 0.001) (Fig. 2A). The DiI-positive BM-MNCs were mostly merged with endothelial marker vWF-positive microvessels (the merge panel in Fig. 2A), while no DiI+ cells were merged in the cardiomyocytes immunostained by cardiac a-myosin heavy chain (data not shown). Interestingly, DiI+ BM-MNCs were found to be attaching onto the endothelium of the microvessel 2 days after US + bubble stimulation (Fig. 2B).

3.3. US + Bubble + BM-MNCs treatment increased the capillary density and prevented cardiac remodeling

Capillary densities (CD) were evaluated by counting ALP+ viable capillaries. We found that the CD of the 20-week-old BIOTO2 hamster were decreased (48 ± 3%, P < 0.005) than the normal (F1B) hamsters and the US + Bubble + BM treatment significantly (P < 0.01) increased the CD (Fig. 3A), whereas there was no significant difference in the CD/myocyte ratio between the treated and untreated BIOTO2 hamsters

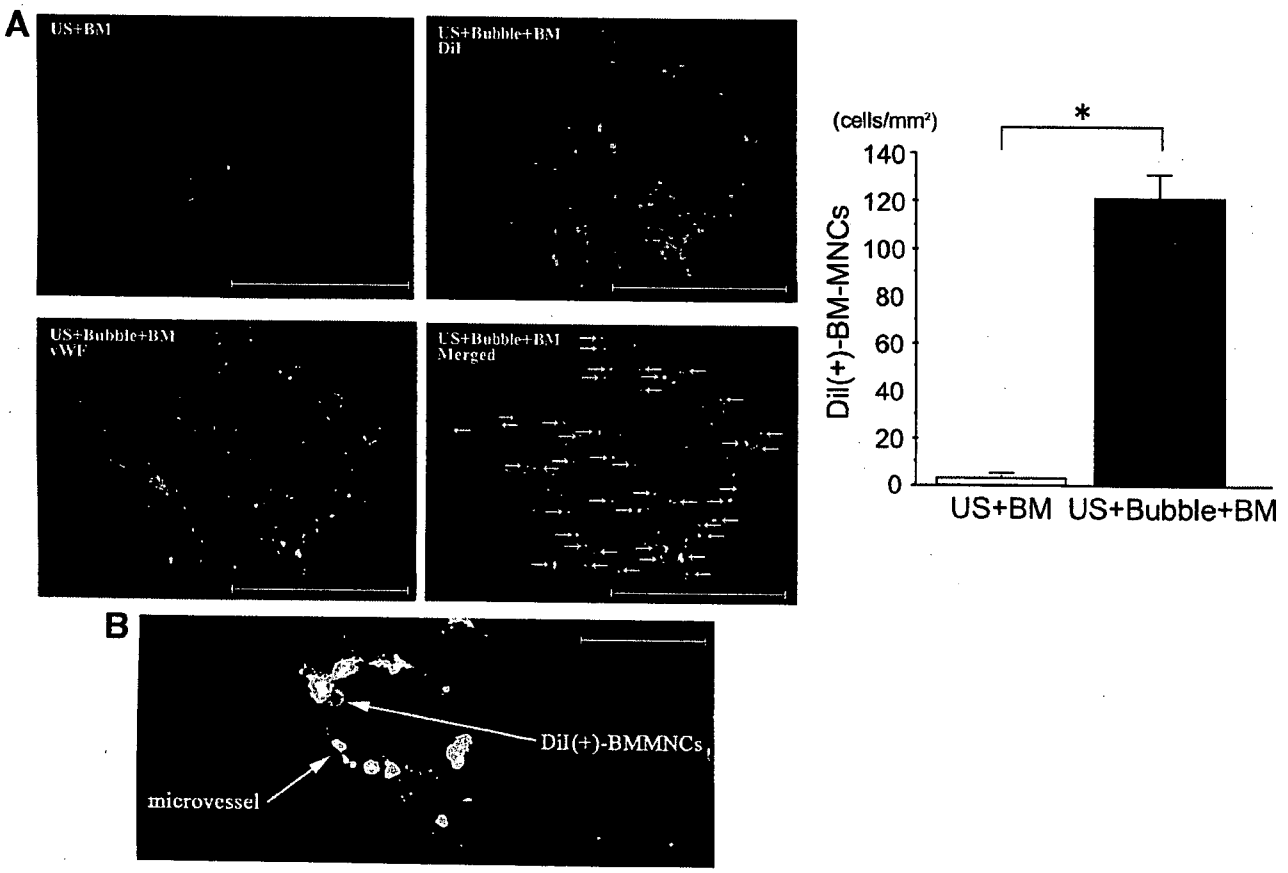

Fig. 2. Fluorescence micrograph of BM-MNCs transplanted by US + Microbubble. (A) US was applied to the anterior chest immediately after intravenous infusion of DiI-labeled BM-MNCs (1 × 10^8 cells) with microbubble (US + Bubble + BM) or without microbubble (US + BM). DiI+ BM-MNCs (red color) and vWF+ microvessels (green color) in the myocardial samples at 14 days after US + Bubble stimulation are shown. Calculated DiI+ cell numbers were significantly higher in US + Bubble + BM group than that in US + BM group (n = 10, *P < 0.001). DiI+ cells mostly corresponded to vWF+ microvessels in the merged image (arrows). Scale bars indicate 200 μm. (B) Attachment of DiI+ BM-MNCs onto the endothelial layer of the microvessel 2 days after US + bubble stimulation. Scale bar indicates 20 μm.

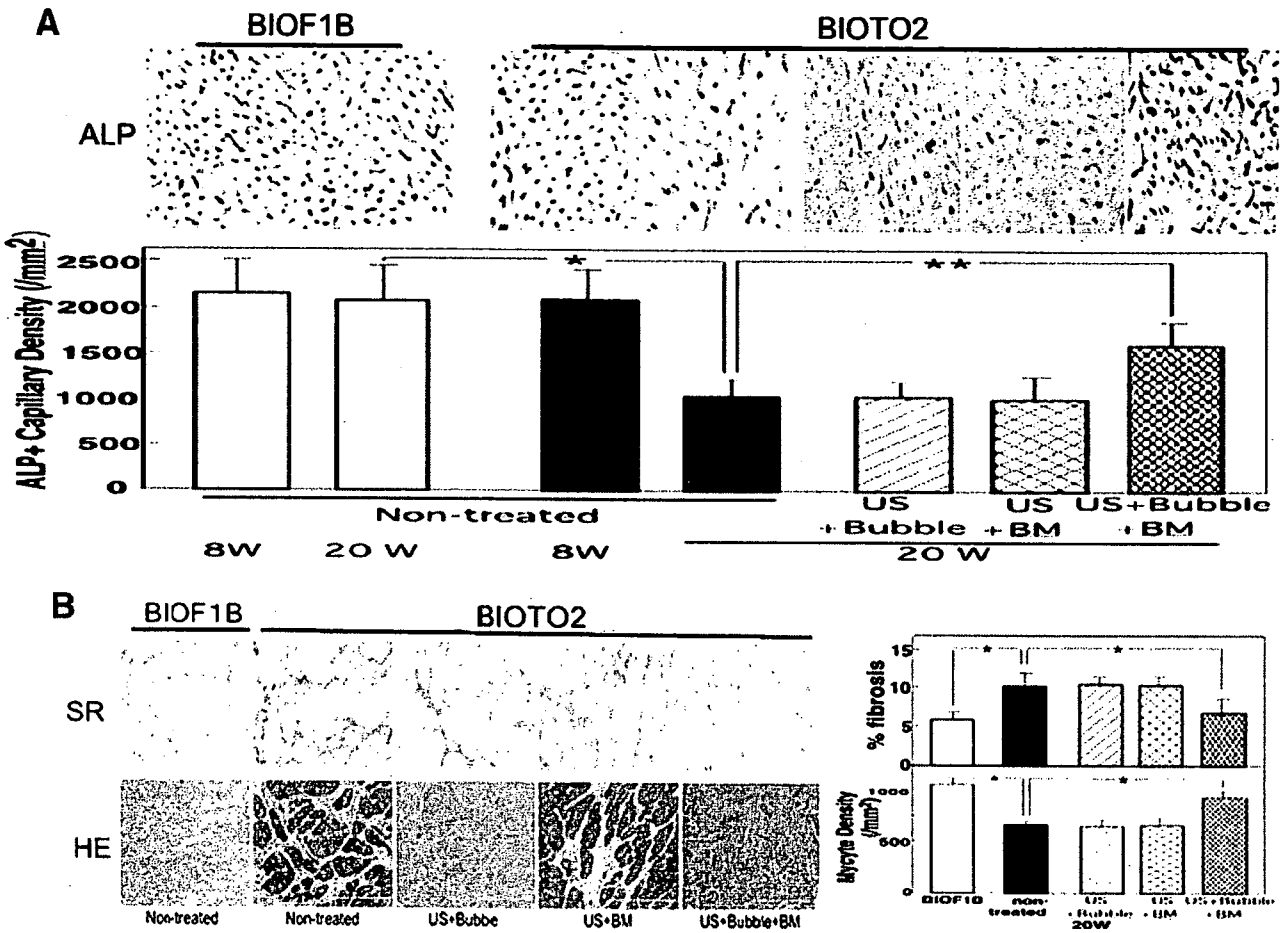

Fig. 3. Histological analysis of myopathic hearts treated with US + microbubble. (A) Evaluation of the capillary density (CD): 8-week-old hamsters were treated with US + microbubble + BM-MNCs infusion (US + Bubble + BM) ($n = 12$), US + microbubble (US + Bubble) ($n = 5$), and US + BM-MNC infusion (US + BM) ($n = 5$) or non-treated ($n = 10$). The LVs of 8- and 20-week-old BIOTO2 or control (BIOF1B) hamsters ($n = 6$) were frozen-sectioned and stained for alkaline phosphatase (ALP), and the number of ALP+ capillaries (blue dots) was counted. Representative images and statistical analysis were shown. $^{*}P < 0.005$, $^{**}P < 0.01$. (B) Evaluation of the cardiac fibrosis and myocyte density: LVs were frozen-sectioned or paraffin-sectioned and stained for Sirius red (SR) or Hematoxylin–Eosin (HE), respectively. Collagen deposition is shown as red color area in SR, while the muscle fibers were stained red in HE. Statistical analysis of the percent fibrosis (fibrotic area ratio to a total microscopic field) and the myocyte density is presented. $^{*}P < 0.01$. Scale bars in panels A and B indicate 200 μm.

(US + Bubble: 1.45 ± 0.15, US + BM: 1.52 ± 0.09, US + Bubble + BM: 1.46 ± 0.08, non-treated: 1.49 ± 0.08, $n = 6$ each). The decrease in myocyte densities in the untreated BIOTO2 hamsters relative to the US + Bubble + BM-treated hamsters (Fig. 3B) may account for the lack of significant difference in the CD/myocyte ratio. The compensatory hypertrophy of remaining cardiomyocytes may be also involved in this discrepancy. Similar findings (the discrepancy between CD and CD/myocyte ratio) were previously reported in the BIOTO2 hamsters [28].

The cardiac fibrosis and myocyte density were evaluated by Sirius red (SR) and Hematoxylin–Eosin (HE) staining,

Table 1
Body weight, ventricular weight, and heart rate data at the age of 20 weeks

	BW (g)	LVW (mg)	LVW/BW (mg/g)	HR (beats/min)
Non-treated ($n = 10$)	99.40 ± 8.859	299.3 ± 12.49	3.037 ± 0.339	308.7 ± 27.11
US + Bubble ($n = 5$)	94.80 ± 4.147	294.8 ± 16.14	3.111 ± 0.158	318.6 ± 24.45
US + BM ($n = 5$)	96.00 ± 12.33	291.2 ± 21.63	3.074 ± 0.462	305.0 ± 28.32
BM + US + Bubble ($n = 12$)	103.7 ± 9.957	$264.1 \pm 15.15^{**,\S,\dagger}$	$2.564 \pm 0.236^{*,\S,\dagger}$	315.8 ± 25.59

Values are means ± SD; control = BIOTO2 treated with intravenous administration of BM-MNCs-free 0.9% saline solution; US + Bubble = BIOTO2 treated with only ultrasound irradiation with microbubble contrast agents administration; BM = BIOTO2 treated with intravenous administration of BM-MNCs without ultrasound irradiation nor microbubble contrast agents administration; BM + US + Bubble = BIOTO2 treated with intravenous administration of BM-MNCs with ultrasound irradiation under microbubble contrast agents administration; BM-MNCs = bone marrow mononuclear cells; BW = body weight; LVW = left ventricular weight; HR = heart rate.

$^{*}P < 0.05$ vs. control; $^{**}P < 0.01$ vs. control; $^{\S}P < 0.05$ vs. US; $^{\dagger}P < 0.05$ vs. BM.

respectively (Fig. 3B). Extensive cardiac fibrosis and the decrease in myocyte density were observed in the untreated myopathic BIOTO2 hamster, as previously described [28]. The fibrosis and myocyte density were significantly recovered 27% and 36% by the US + Bubble + BM treatment, respectively (Fig. 3B). The number of the apoptotic cells in the US + Bubble + BM group was 23% less than the non-treated control group (0.53 ± 0.12, $n = 12$ vs. $0.69 \pm 0.01/mm^2$, $n = 10$, $P < 0.01$). LV weight of myopathic hamsters treated by the US + Bubble + BM-MNCs was decreased ~17.5% ($P < 0.01$) compared with those in the non-treated control, US + Bubble alone or BM injection groups (Table 1). Thus, BM-MNCs transplanted by the US + Bubble stimulation enhance neovessel formation in myopathic hearts and inhibited the cardiac remodeling, including interstitial fibrosis and cell apoptosis.

3.4. Increase in blood perfusion improved the cardiac function in the US + Bubble + BM-treated heart

Regional blood perfusion was evaluated by ^{99m}Tc-Tetrofosmin scintigraphy (Fig. 4A). The ^{99m}Tc-Tetrofosmin uptake was decreased all over the untreated myopathic heart, whereas the distribution of radioactivity was homogenously increased in the US + Bubble + BM-MNC infusion group and the total dosed radioactivity (% uptake) of ^{99m}Tc-Tetrofosmin was 1.2-fold greater ($n = 5$, $P < 0.01$) than that in the non-treated group (Fig. 4A, right panel). Thus, US + Bubble + BM-MNC treatment was shown to actually increase the regional blood perfusion in the myopathic hamster heart.

To examine the in vivo consequence of improvement of myocardial blood perfusion by US + Bubble + BM-MNC treatment, we analyzed the cardiac function, LV diastolic

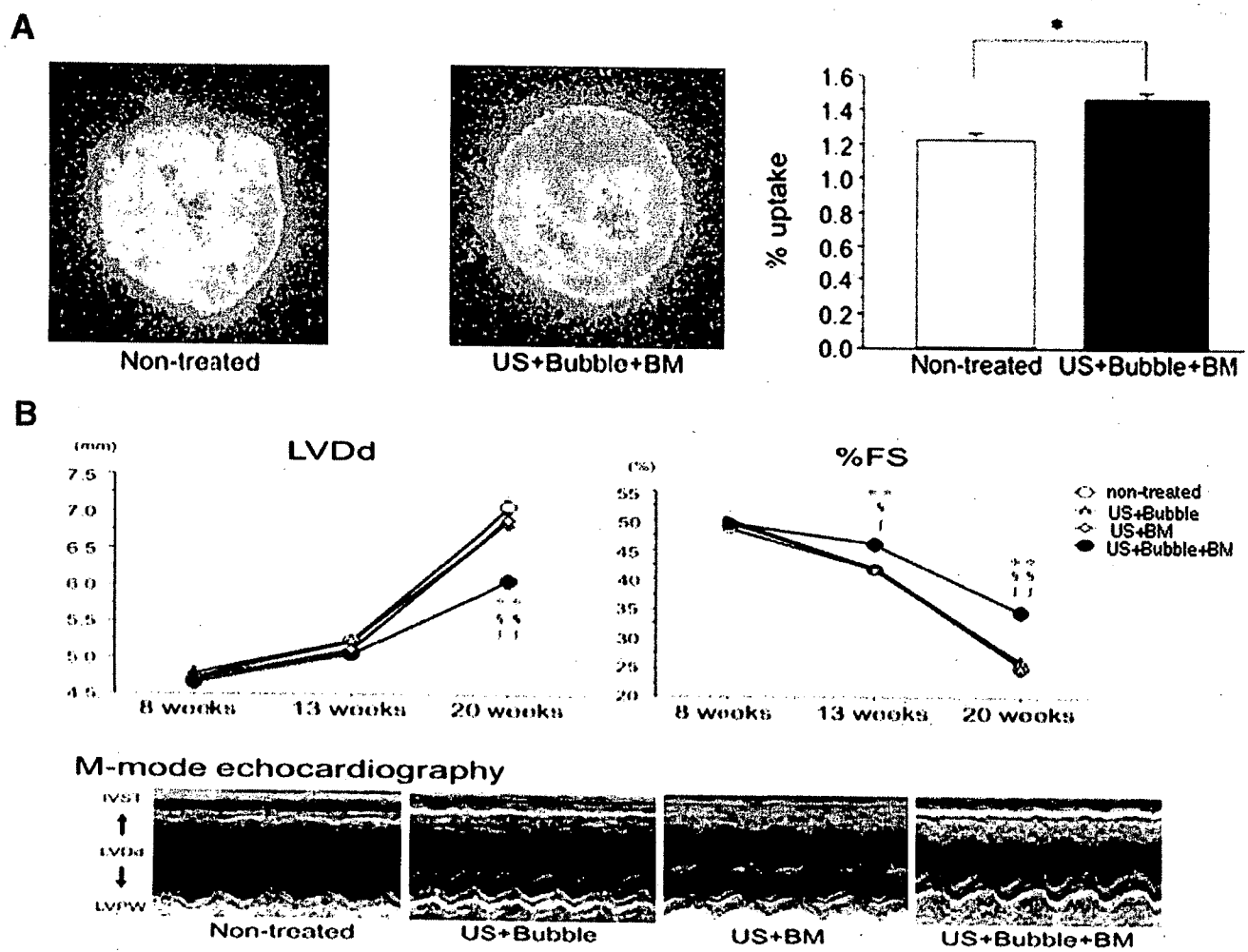

Fig. 4. Increase in blood perfusion improves the cardiac function of US + Bubble + BM-treated cardiomyopathy hamster. (A) Blood perfusion in the myocardium was evaluated by ^{99m}Tc-Tetrofosmin scintigraphy 12 weeks after US + microbubble + BM-MNCs infusion (US + Bubble + BM). Yellow and orange color indicate lower and higher blood perfusion, respectively. Myocardial ^{99m}Tc-Tetrofosmin uptake relative to the total dosed radioactivity (percent uptake) is evaluated in the right panel. The percent uptake was 1.2-fold higher ($n = 5$, $P < 0.01$) in the US + Bubble + BM-treated hamsters than in the non-treated group. $^{*}P < 0.01$ vs. non-treated control. (B) Evaluation of LV function by echocardiography. BIOTO2 hamsters (8-week-old) were treated with US + Bubble, US + BM, and US + Bubble + BM. LV functions were evaluated on Weeks 8, 13, and 20. Representative images on Week 20 are shown in the lower panel. The LV diastolic diameter (LVDd), fractional shortening (%FS), intra-ventricular septum (IVST), left ventricular posterior wall (LVPW), $^{**}P < 0.01$ vs. non-treated, $^{\S}P < 0.05$ vs. US + Bubble, $^{\S\S}P < 0.01$ vs. US + Bubble, $^{\dagger}P < 0.05$ vs. US + BM, $^{\dagger\dagger}P < 0.01$ vs. US + BM.

diameter (LVDd), and fractional shortening (%FS) by echocardiography on Weeks 8, 13, and 20 after treatment in the non-treated control, US + Bubble-, US + BM-MNCs-, and US + Bubble + BM-MNCs-treated groups (Fig. 4B). All parameters of Week 8 were not significantly different between each group. On Week 13, there were no significant differences in LVDd among each group, while %FS in the US + Bubble + BM-MNCs group was appreciably improved (11.1 ± 0.1%, $P < 0.05$) compared with the non-treated control, and the effect was more apparent at Week 20 (40.2 ± 0.2%, $P < 0.01$). At Week 20, the LVDd in the US + Bubble + BM-MNC group was also significantly improved over the control (18.4 ± 0.2%, $P < 0.01$). There were no changes in the LVDd and %FS between the non-treated control, US + Bubble, and US + BM-MNC treatment groups. Consistent with these parameters, the motion dynamics of the posterior wall and septum were apparently improved in US + Bubble + BM-MNC group (Fig. 4B, lower panel).

3.5. Expression of angiogenic growth factors by the transplanted BM-MNCs

We previously reported that BM-MNCs produce VEGF and bFGF that play a major role in the induction of neocapillary formation after BM-MNCs implantation into ischemic limbs [5,30] and myocardium [31]. We therefore examined the expression of VEGF and bFGF in the myopathic hearts in which BM-MNCs were transplanted by US + Bubble. Western blot analysis revealed that US + Bubble + BM-MNCs treatment markedly increased the expression of VEGF and bFGF ($P < 0.001$, 2.6-fold and 2.3-fold, respectively) compared with the non-treated control, while neither US + BM-MNCs nor the US + Bubble-treated groups showed significant changes (Fig. 5).

3.6. Induction of adhesion molecules and inflammatory cytokines by US + Bubble treatment

We next examined the possibility that US + Bubble treatment stimulates the expression of the adhesion molecules, causing the adhesion of transfused BM-MNCs or monocyte/macrophage onto the endothelial layer, as observed in Fig. 2B. Western blotting showed that the expressions of the adhesion molecules VCAM-1 and ICAM-1 increased to ~2.5-fold ($P < 0.01$) in the US + Bubble- or US + Bubbles + BM-MNCs-treated myocardium compared with the non-treated control, whereas only Bubble- or only US-treated groups did not induce the significant expression (Fig. 6A). To study the tissue localization of the adhesion molecules and monocyte/macrophages (CD68), we performed the immunohistochemical analysis. As the anti-hamster antibodies positive for VCAM-1, ICAM-1, and CD68 were not available, we prepared the rat myocardial samples 3 days after US + Bubble treatment and used the anti-rat antibodies for immunostaining. We found that the expressions of VCAM-1 and ICAM-1 were localized in the vWF+ vessels in the US + Bubble-treated myocardium (Fig. 6B, ICAM-1 not shown), whereas no expression was observed in the untreated

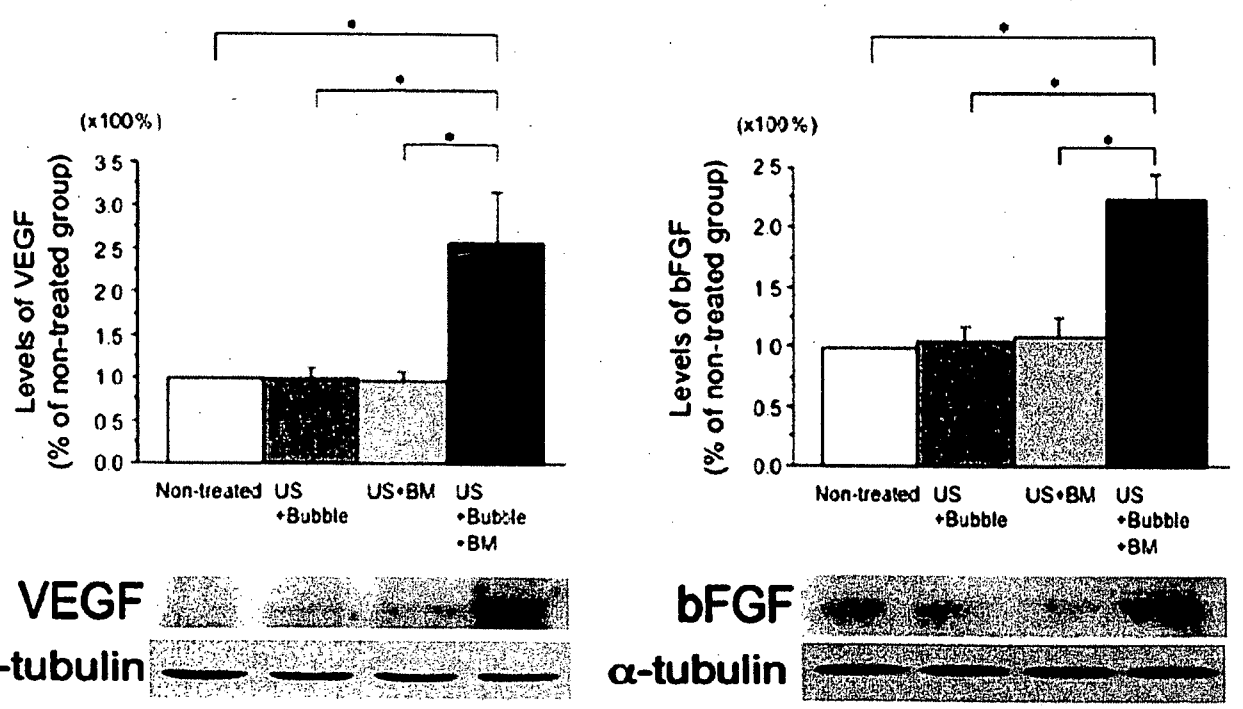

Fig. 5. Expression of angiogenic growth factors. Three days after US + BM, US + Bubble, or US + Bubble + BM treatment ($n = 5$, each), LV lysates were immunoblotted with the anti-VEGF, anti-basic FGF (bFGF), and anti-α-tubulin antibodies. The signal densities of VEGF and bFGF were arbitrarily normalized by that of α-tubulin. *$P < 0.001$.

control (Fig. 6C). The CD68+ macrophages were markedly infiltrated in the US + Bubble-treated myocardium (Fig. 6C, left panel), in which CD68+ cells mainly adhered onto the inner lumen of VCAM-1+ vessels and were partly observed in the interstitial region around the vessels (Fig. 6C, right panel), suggesting that the induction of the adhesion molecules in the US + Bubble-treated vessels caused the infiltration of macrophages into the interstitial region of myocardium.

We also examined the expression of TNF-α, IL-1β, and MCP-1 by the real-time PCR and immunohistochemical analysis. As the anti-hamster antibodies positive for MCP-1, TNF-α, and IL-1β were not available, we prepared the rat myocardial samples 3 days after US + Bubble treatment and used the anti-rat antibodies for immunostaining. The real-time PCR showed that their expressions are markedly elevated (approximately 7- to 15-fold, $P < 0.001$) compared with those in the non-treated control (Fig. 7A). The immunohistochemical analysis revealed that these cytokines (MCP-1, TNF-α, and IL-1β) were mainly expressed in the vessels in the US + Bubble-treated myocardium (Fig. 7B).

4. Discussion

A new delivery system of drugs or genes has been developed using US-targeted microbubble destruction. The drugs or genes that attach onto gas-filled microbubbles circulate through the intravascular space and are mechanically destroyed within the target organ by US [18,19,21,32], whereas no studies have been reported that determine whether this method is feasible for delivering the "vascular progenitor cells" to specific vascular sites. US-targeted microbubble destruction was reported to have an inflammatory action on

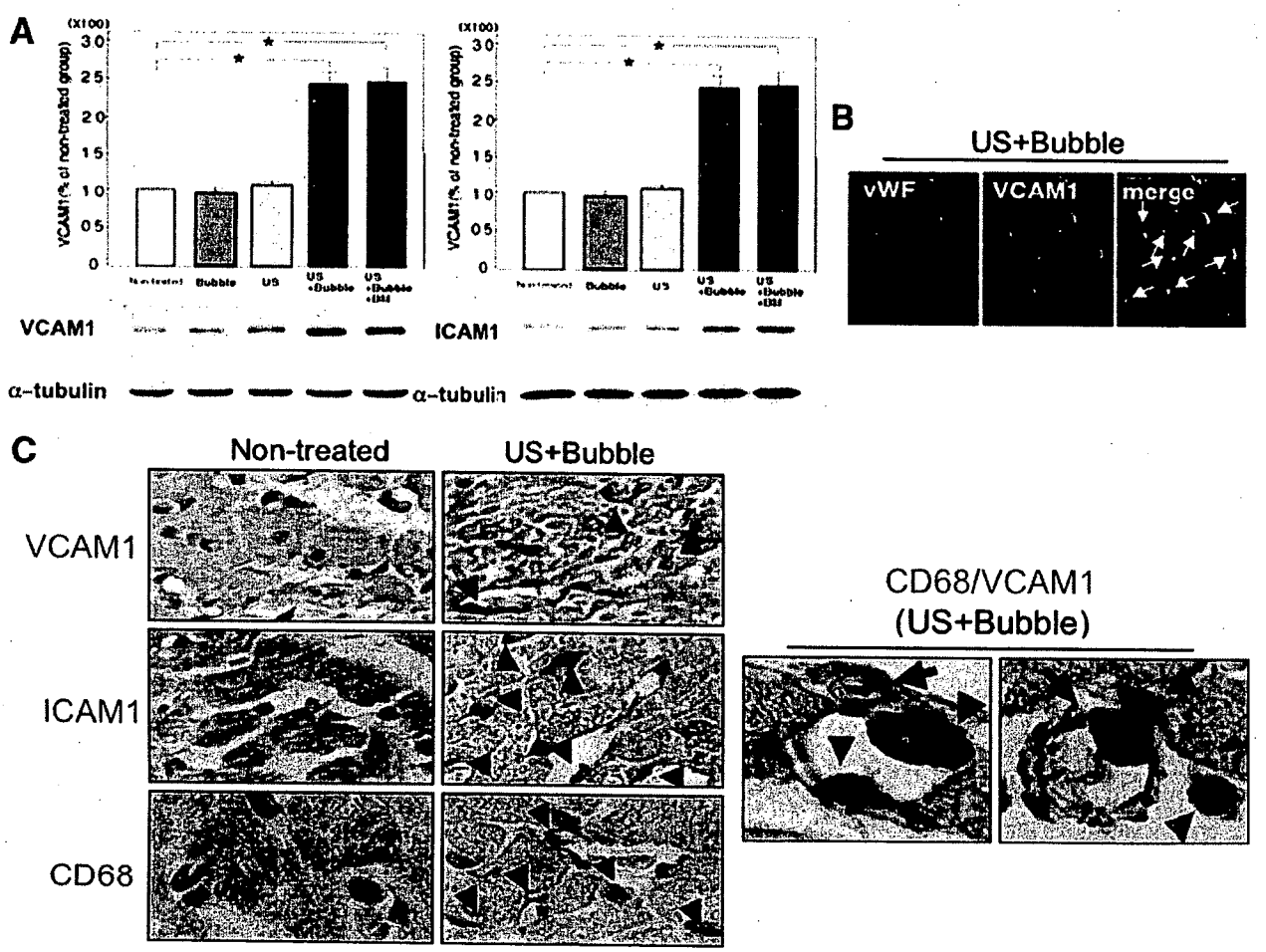

Fig. 6. Expression of adhesion molecules in US + Bubble-treated heart. (A) Two days after Bubble alone, US alone, US + Bubble, or US + Bubble + BM treatment, LV lysates were subjected to the immunoblot analysis using anti-VCAM-1, anti-ICAM-1, and anti-α-tubulin antibodies. Signal densities of VCAM-1 and ICAM-1 were arbitrarily normalized by α-tubulin. The expression of VCAM-1 and ICAM-1 was significantly (*$P < 0.01$) increased to 2.3- and 2.2-fold to compared the non-treated control, respectively. (B) For immunohistochemistry, we used the rat model as the hamster antibodies were not available. Frozen-sectioned rat LV samples (3 days after US + Bubble treatment) were immunostained with anti-rat vWF and anti-rat VCAM-1 antibodies followed by Rhodamin- or FITC-labeled secondary antibodies. VCAM-1 positive cells mostly corresponded to vWF positive vessels. Scale bar indicates 200 μm. (C) Two days after US + Bubble treatment, paraffin-sectioned rat LVs were immunostained using the antibodies against rat VCAM-1, ICAM-1, or CD68 (macrophage-specific antigen) with DAB or naphtol, respectively. Arrowheads in panel C, left panels indicate the VCAM-1+ or ICAM-1+ capillaries and CD68+ cells. Double fluorescence images using anti-rat CD68− and anti-rat VCAM-1− antibodies are presented in the right panels. CD68+ cells (red arrowheads) mainly adhered onto the inner lumen of VCAM-1+ vessels (brown arrows) or were partly observed in the interstitial region around the vessels.

the cell surface by making small holes that revert to a normal appearance within 24 h [13]. Song et al. [14,23] reported that US-targeted microbubble destruction causes capillary rupturing that stimulates neovessel formation and an increase in blood flow in both normal and ischemic skeletal muscles. We previously demonstrated that the recruitment of BM-MNCs stimulates angiogenesis in ischemic muscles by releasing angiogenic factors, including VEGF or bFGF and by the supply of endothelial progenitors [29,30]. Furthermore, we reported that BM-MNCs had a higher adhesive activity on the endothelium than did peripheral blood MNCs, and this adhesive activity was dependent on the expression level of adhesion molecules on the endothelium [29]. We therefore expanded the previous studies by Song et al. [14,23] and further studied whether US-mediated microbubble destruction, combined with the intravenous transfusion of BM-MNCs, enhanced neovessel formation by an increase in the endothelial attachment of BM-MNCs, leading to improvement in blood perfusion and cardiac function of BIOTO2 cardiomyopathy caused by limited neocapillary formation [26–28]. The present study demonstrates for the first time that this novel cell delivery system enables the vascular-endothelium-targeted attachment of infused BM-MNCs and increases the neovessel formation and blood flow in myopathic hearts, resulting in an improvement of cardiac function via the inhibition of myocyte apoptosis and interstitial fibrosis. This functional recovery was not found by BM-MNCs transfusion without US + Bubble, suggesting that US + Bubble-mediated BM-MNCs delivery is highly potent for neovascularization.

US + Bubble stimulation was reported to mechanically induce pores in the capillary wall [16]. The present study showed that the expression of adhesion molecules was markedly induced by the US + Bubble-mediated response (Fig. 5) and transfused BM-MNCs actually attached onto the injured endothelial layer (Fig. 2A). The adhesion activity of BM-MNCs on the endothelial layer was reported to be markedly higher than that of the circulating MNCs, and its adhesive activity was enhanced on the balloon-injured endothelium [29]. Indeed, as we observed in Fig. 2A, BM-MNCs infusion with US + Bubble stimulation achieved much more efficient regional cell delivery than simple BMC injection. Transplantation of autologous BM-MNCs has been clinically applied for patients with ischemic heart diseases via catheter-based approaches, direct injection into the ischemic myocardium [11,12,33], or intracoronary infusion [6–9]. Although they showed favorable effects on cardiac remodeling and function, the efficiency of cell delivery was still limited and such therapies were invasive. Most of the injected BM-derived mesenchymal stem cells died 4 days after intramyocardial injection [34], and ~60% of the BM-MNCs infused by intracoronary injection were trapped by the spleen and liver, and a minor population of cells (~10%) were present in the heart [35]. We only found a transient appearance of ventricular premature beats during the 90 s of US + Bubble application, and thereafter no incidences of death were observed during the observation period in any of the treated myopathic hamsters (n = 48). Thus, the present study suggests that US + Bubble + BM-MNC treatment is a

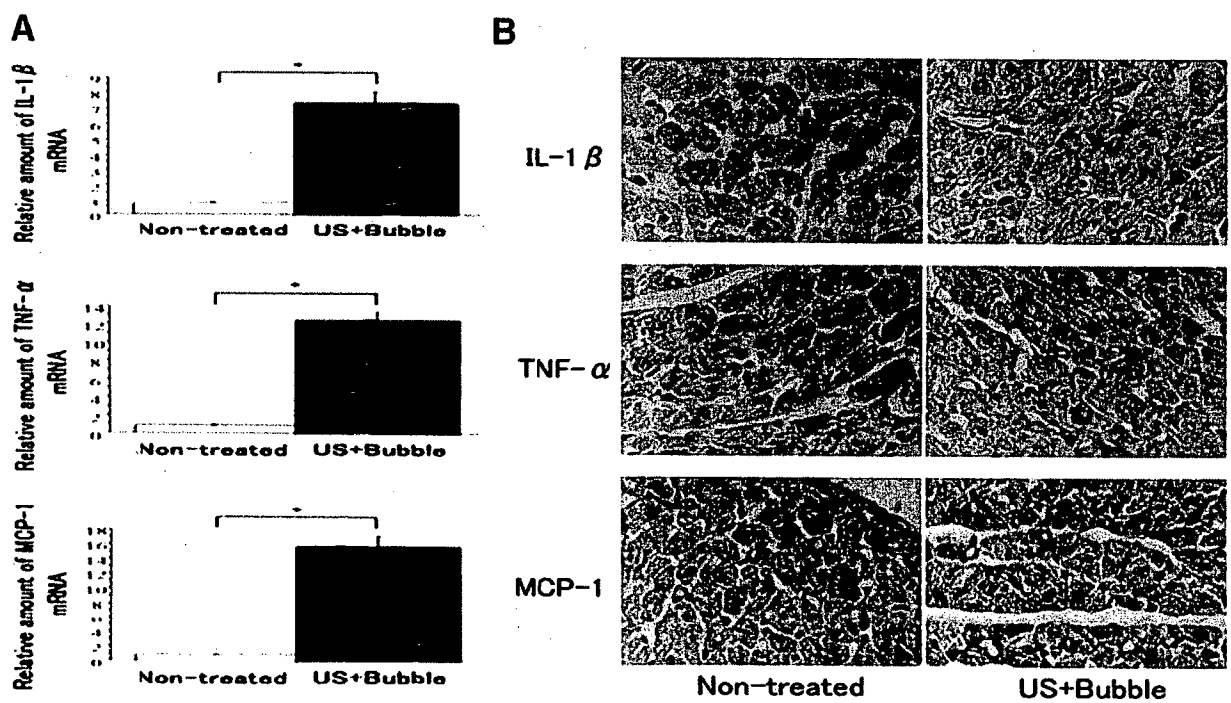

Fig. 7. US + Bubble induced the expression of inflammatory chemokine and cytokines. (A) Three days after US + Bubble treatment, total RNAs of rat LVs were subjected to the real-time PCR analysis for expression of IL-1β, TNF-α, and MCP1. Their mRNA levels in the US + Bubble-treated myocardium were significantly (*$P < 0.001$, $n = 5$ each) higher than those in the non-treated groups. (B) Rat LVs were also paraffin-sectioned and immunostained using the antibodies against rat IL-1β, rat TNF-α, and rat MCP-1. Brown dot indicates the positive cells.

safe and feasible non-invasive system for targeted cell delivery to the myocardium.

We found the adhesion of transfused BM-MNCs and the increased expressions of adhesion molecules on the US + Bubble-stimulated endothelium (Fig. 5). Considering our recent study reporting that systemically transplanted BM-MNCs can be firmly attached onto the injured vascular endothelium in an adhesive molecule-dependent manner [29], it is likely that the mechanical impact of US-mediated microbubble destruction induces the up-regulation of these adhesion molecules on the targeted vascular endothelium, causing the attachment of transfused BM-MNCs onto targeted endothelial layer. The present study clearly shows that endothelial progenitors included in BM-MNCs trans-differentiate to endothelial-like cells (Fig. 2) to repair US + Bubble-stimulated endothelium as well as supply the angiogenic factors (VEGF and bFGF) (Fig. 4) for neovessel formation. BM-MNC-derived endothelial progenitors that attached on the endothelial layer or leaked out from the injured endothelium may be incorporated into the regenerated endothelium and/or stimulate neovessel formation by supplying angiogenic factors. Thus, these synergistic bioeffects after US + Bubble + BM-MNC stimulation likely induced a potent angiogenic response in the US + microbubble-applied myocardium.

Although there is a concern that the US application to the anterior chest may cause the geometrical unevenness of the biological effects in the LV wall, there was no obvious difference in the biological effect between the anterior and the inferior LV wall in the US + Bubble + BM-treated heart, such as the CD (1354 ± 222.4 and 1288 ± 207.2/mm^2, n = 5) or the cardiac muscle fiber density (926.3 ± 88.7 and 901.3 ± 66.8/mm^2, n = 5). The diameter of the US probe (approximately 3 cm) is much bigger than the size of the hamster's heart (less than 1 cm), and furthermore the US was applied from various directions with continuously changing the angle to the chest wall, leading to achievement of the geometrically even biological effect all over the field of the myocardium.

The BIOTO2 Syrian hamsters used in this study inherit cardiomyopathy in an autosomal recessive manner and manifested dilated cardiomyopathy [36,37]. They have a genetic mutation of sarcoglycans, a subcomplex of the dystrophin-associated glycoprotein complex (DAGC) [38–40]. The impairment of the cardiac function in this hamster was caused by altered microvasculature, leading to a decrease in cardiac blood blow [26,28]. The BIOTO2 hamster exhibited a significantly lower capillary density [28] that correlated with the myocyte density and cardiac function. Angiogenetic gene therapy using hepatic growth factor was shown to enhance the angiogenic response and improve blood perfusion in the other myopathic hamster BIO14.6 model [24]. Combined with our present result using angiogenic cell therapy, it is likely that the enhancement of neovessel formation followed by an increase in regional blood flow inhibits cardiac remodeling in myopathic hearts and improves heart failure. Conclusively, BM-MNCs transplantation by US–microbubble-mediated cell delivery is a novel approach for an efficient angiogenic cell therapy, which is the most relevant strategy for the treatment of idiopathic myopathic hearts that requires an extensive cell delivery to the myocardium.

Acknowledgments

This study was supported in part by research grants from the Ministry of Education, Science, Sports and Culture, and the Ministry of Health, Labor and Welfare, Japan, the Study Group of Molecular Cardiology, the Japan Medical Association, and the Japan Heart Foundation.

References

[1] Asahara T, Murohara T, Sullivan A, Silver M, van der Zee R, Li T, et al. Isolation of putative progenitor endothelial cells for angiogenesis. Science 1997;275:964–7.

[2] Asahara T, Masuda H, Takahashi T, Kalka C, Pastore C, Silver M, et al. Bone marrow origin of endothelial progenitor cells responsible for postnatal vasculogenesis in physiological and pathological neovascularization. Circ Res 1999;85:221–8.

[3] Kalka C, Masuda H, Takahashi T, Kalka-Moll WM, Silver M, Kearney M, et al. Transplantation of ex vivo expanded endothelial progenitor cells for therapeutic neovascularization. Proc Natl Acad Sci U S A 2000; 97:3422–7.

[4] Murohara T, Ikeda H, Duan J, Shintani S, Sasaki K, Eguchi H, et al. Transplanted cord blood-derived endothelial precursor cells augment postnatal neovascularization. J Clin Invest 2000;105:1527–36.

[5] Tateishi-Yuyama E, Matsubara H, Murohara T, Ikeda U, Shintani S, Masaki H, et al, Therapeutic Angiogenesis using Cell Transplantation (TACT) Study Investigators. Therapeutic angiogenesis for patients with limb ischaemia by autologous transplantation of bone-marrow cells: a pilot study and a randomised controlled trial. Lancet 2002;360:427–35.

[6] Assmus B, Schachinger V, Teupe C, Britten M, Lehmann R, Dobert N, et al. Transplantation of progenitor cells and regeneration enhancement in acute myocardial infarction (TOPCARE-AMI). Circulation 2002;106: 3009–17.

[7] Britten MB, Abolmaali ND, Assmus B, Lehmann R, Honold J, Schmitt J, et al. Infarct remodeling after intracoronary progenitor cell treatment in patients with acute myocardial infarction (TOPCARE-AMI): mechanistic insights from serial contrast-enhanced magnetic resonance imaging. Circulation 2003;108:2212–8.

[8] Schachinger V, Assmus B, Britten MB, Honold J, Lehmann R, Teupe C, et al. Transplantation of progenitor cells and regeneration enhancement in acute myocardial infarction: final one-year results of the TOPCARE-AMI trial. J Am Coll Cardiol 2004;44:1690–9.

[9] Wollert KC, Meyer GP, Lotz J, Ringes-Lichtenberg S, Lippolt P, Breidenbach C, et al. Intracoronary autologous bone-marrow cell transfer after myocardial infarction: the BOOST randomised controlled clinical trial. Lancet 2004;364:141–8.

[10] Fuchs S, Satler LF, Kornowski R, Okubagzi P, Weisz G, Baffour R, et al. Catheter-based autologous bone marrow myocardial injection in no-option patients with advanced coronary artery disease: a feasibility study. J Am Coll Cardiol 2003;41:1721–4.

[11] Tse HF, Kwong YL, Chan JK, Lo G, Ho CL, Lau CP. Angiogenesis in ischaemic myocardium by intramyocardial autologous bone marrow mononuclear cell implantation. Lancet 2003;361:47–9.

[12] Perin EC, Dohmann HF, Borojevic R, Silva SA, Sousa AL, Mesquita CT, et al. Transendocardial, autologous bone marrow cell transplantation for severe, chronic ischemic heart failure. Circulation 2003;107:2294–302.

[13] Skyba DM, Price RJ, Linka AZ, Skalak TC, Kaul S. Direct in vivo visualization of intravascular destruction of microbubbles by ultrasound and its local effects on tissue. Circulation 1998;98:290–3.

[14] Song J, Cottler PS, Klibanov AL, Kaul S, Price RJ. Microvascular remodeling and accelerated hyperemia blood flow restoration in arterially

occluded skeletal muscle exposed to ultrasonic microbubble destruction. Am J Physiol, Heart Circ Physiol 2004;287:H2754–61.
[15] Price RJ, Skyba DM, Kaul S, Skalak TC. Delivery of colloidal particles and red blood cells to tissue through microvessel ruptures created by targeted microbubble destruction with ultrasound. Circulation 1998; 98:1264–7.
[16] Song J, Chappell JC, Qi M, VanGieson EJ, Kaul S, Price RJ. Influence of injection site, microvascular pressure, and ultrasound variables on microbubble-mediated delivery of microspheres to muscle. J Am Coll Cardiol 2002;39:726–31.
[17] Ay T, Havaux X, Van Camp G, Campanelli B, Gisellu G, Pasquet A, et al. Destruction of microbubbles by ultrasound: effects on myocardial function, coronary perfusion pressure, and microvascular integrity. Circulation 2001;104:461–6.
[18] Taniyama Y, Tachibana K, Hiraoka K, Namba T, Yamasaki K, Hashiya N, et al. Local delivery of plasmid DNA into rat carotid artery using ultrasound. Circulation 2002;105:1233–9.
[19] Teupe C, Richter S, Fisslthaler B, Randriamboavonjy V, Ihling C, Fleming I, et al. Vascular gene transfer of phosphomimetic endothelial nitric oxide synthase (S1177D) using ultrasound-enhanced destruction of plasmid-loaded microbubbles improves vasoreactivity. Circulation 2002;105:1104–9.
[20] Mukherjee D, Wong J, Griffin B, Ellis SG, Porter T, Sen S, et al. Ten-fold augmentation of endothelial uptake of vascular endothelial growth factor with ultrasound after systemic administration. J Am Coll Cardiol 2000; 35:1678–86.
[21] Price RJ, Kaul S. Contrast ultrasound targeted drug and gene delivery: an update on a new therapeutic modality. J Cardiovas Pharmacol Ther 2002;7:171–80.
[22] Shohet RV, Chen S, Zhou YT, Wang Z, Meidell RS, Unger RH, et al. Echocardiographic destruction of albumin microbubbles directs gene delivery to the myocardium. Circulation 2000;101:2554–6.
[23] Song J, Qi M, Kaul S, Price RJ. Stimulation of arteriogenesis in skeletal muscle by microbubble destruction with ultrasound. Circulation 2002; 106:1550–5.
[24] Taniyama Y, Morishita R, Aoki M, Hiraoka K, Yamasaki K, Hashiya N, et al. Angiogenesis and antifibrotic action by hepatocyte growth factor in cardiomyopathy. Hypertension 2002;40:47–53.
[25] Kondo I, Ohmori K, Oshita A, Takeuchi H, Fuke S, Shinomiya K, et al. Treatment of acute myocardial infarction by hepatocyte growth factor gene transfer: the first demonstration of myocardial transfer of a "functional" gene using ultrasonic microbubble destruction. J Am Coll Cardiol 2004;44:644–53.
[26] Factor SM, Minase T, Cho S, Dominitz R, Sonnenblick EH. Microvascular spasm in the cardiomyopathic Syrian hamster: a preventable cause of focal myocardial necrosis. Circulation 1982;66:342–54.
[27] Iwata Y, Katanosaka Y, Arai Y, Komamura K, Miyatake K, Shigekawa M. A novel mechanism of myocyte degeneration involving the Ca^{2+}-permeable growth factor-regulated channel. J Cell Biol 2003;161:957–67.
[28] Shimizu T, Okamoto H, Watanabe M, Kumamoto H, Chiba S, Matsui Y, et al. Altered microvasculature is involved in remodeling processes in cardiomyopathic hamsters. Jpn Heart J 2003;44:111–26.
[29] Fujiyama S, Amano K, Uehira K, Yoshida M, Nishiwaki Y, Nozawa Y, et al. Bone marrow monocyte lineage cells adhere on injured endothelium in a monocyte chemoattractant protein-1-dependent manner and accelerate reendothelialization as endothelial progenitor cells. Circ Res 2003;93:980–9.
[30] Iba O, Matsubara H, Nozawa Y, Fujiyama S, Amano K, Mori Y, et al. Angiogenesis by implantation of peripheral blood mononuclear cells and platelets into ischemic limbs. Circulation 2002;106:2019–25.
[31] Kamihata H, Matsubara H, Nishiue T, Fujiyama S, Tsutsumi Y, Ozono R, et al. Implantation of bone marrow mononuclear cells into ischemic myocardium enhances collateral perfusion and regional function via side supply of angioblasts, angiogenic ligands, and cytokines. Circulation 2001;104:1046–52.
[32] Bekeredjian R, Chen S, Frenkel PA, Grayburn PA, Shohet RV. Ultrasound-targeted microbubble destruction can repeatedly direct highly specific plasmid expression to the heart. Circulation 2003;108:1022–6.
[33] Perin EC, Dohmann HF, Borojevic R, Silva SA, Sousa AL, Silva GV, et al. Improved exercise capacity and ischemia 6 and 12 months after transendocardial injection of autologous bone marrow mononuclear cells for ischemic cardiomyopathy. Circulation 2004;110(11 Suppl 1):II213–8.
[34] Toma C, Pittenger MF, Cahill KS, Byrne BJ, Kessler PD. Human mesenchymal stem cells differentiate to a cardiomyocyte phenotype in the adult murine heart. Circulation 2002;105:93–8.
[35] Siminiak T, Czepeczynski R, Grygieska B, et al. Evidence for extravasation of intracoronary administered bone-marrow derived CD34+ stem cells in patients with acute myocardial infarction. Circulation 2004;110:III-51.
[36] Homburger F, Baker JR, Nixon CW, Wilgram G. New hereditary disease of Syrian hamsters. Primary, generalized polymyopathy and cardiac necrosis. Arch Intern Med 1962;110:660–2.
[37] Jasmin G, Eu HY. Cardiomyopathy of hamster dystrophy. Ann NY Acad Sci 1979;317:46–58.
[38] Roberds SL, Ervasti JM, Anderson RD, Ohlendieck K, Kahl SD, Zoloto D, et al. Disruption of the dystrophin–glycoprotein complex in the cardiomyopathic hamster. J Biol Chem 1993;268:11496–9.
[39] Sakamoto A, Ono K, Abe M, Jasmin G, Eki T, Murakami Y, et al. Both hypertrophic and dilated cardiomyopathies are caused by mutation of the same gene, -sarcoglycan, in hamster: an animal model of disrupted dystrophin-associated glycoprotein complex. Proc Natl Acad Sci U S A 1997;94:13873–8.
[40] Panchal BC, Trippodo NC. Systemic and regional haemodynamics in conscious Bio TO-2 cardiomyopathic hamsters. Cardiovasc Res 1993;27:2264–9.

Circulation Research

JOURNAL OF THE AMERICAN HEART ASSOCIATION

American Heart Association®

Learn and Live℠

Erythropoietin-Mobilized Endothelial Progenitors Enhance Reendothelialization via Akt-Endothelial Nitric Oxide Synthase Activation and Prevent Neointimal Hyperplasia

Norifumi Urao, Mitsuhiko Okigaki, Hiroyuki Yamada, Yasushi Aadachi, Kuniharu Matsuno, Akihiro Matsui, Shinsaku Matsunaga, Kento Tateishi, Tetsuya Nomura, Tomosaburo Takahashi, Tetsuya Tatsumi and Hiroaki Matsubara

Circ. Res. 2006;98;1405-1413; originally published online Apr 27, 2006;
DOI: 10.1161/01.RES.0000224117.59417.f3
Circulation Research is published by the American Heart Association. 7272 Greenville Avenue, Dallas, TX 72514
 Print ISSN: 0009-7330. Online ISSN: 1524-4571

Erythropoietin-Mobilized Endothelial Progenitors Enhance Reendothelialization via Akt–Endothelial Nitric Oxide Synthase Activation and Prevent Neointimal Hyperplasia

Norifumi Urao, Mitsuhiko Okigaki, Hiroyuki Yamada, Yasushi Aadachi, Kuniharu Matsuno, Akihiro Matsui, Shinsaku Matsunaga, Kento Tateishi, Tetsuya Nomura, Tomosaburo Takahashi, Tetsuya Tatsumi, Hiroaki Matsubara

Abstract—We investigated whether the mobilization of endothelial progenitor cells (EPCs) by exogenous erythropoietin (Epo) promotes the repair of injured endothelium. Recombinant human Epo was injected (1000 IU/kg for the initial 3 days) after wire injury of the femoral artery of mice. Neointimal formation was inhibited by Epo to 48% of the control ($P<0.05$) in an NO-dependent manner. Epo induced a 1.4-fold increase in reendothelialized area of day 14 denuded vessels, 55% of which was derived from bone marrow (BM) cells. Epo increased the circulating Sca-1$^+$/Flk-1$^+$ EPCs (2.0-fold, $P<0.05$) with endothelial properties NO dependently. BM replacement by GFP- or β-galactosidase–overexpressing cells showed that Epo stimulated both differentiation of BM-derived EPCs and proliferation of resident ECs. BM-derived ECs increased 2.2- to 2.7-fold ($P<0.05$) in the Epo-induced neoendothelium, where the expression of Epo receptor was upregulated. Epo induced Akt/eNOS phosphorylation and NO synthesis on EPCs and exerted an antiapoptotic action on wire-injured arteries. In conclusion, Epo treatment inhibits the neointimal hyperplasia after arterial injury in an NO-dependent manner by acting on the injured vessels and mobilizing EPCs to the neo-endothelium. **(*Circ Res*. 2006;98:1405-1413.)**

Key Words: restenosis ■ endothelium ■ progenitor cells ■ erythropoietin

Endothelial cells (ECs) cover the luminal surface of blood vessels and maintain multiple vascular functions. Disruption of endothelial coverage causes a decrease in the production of vasculoprotective mediators such as nitric oxide (NO), leading to elevated vascular tonus, enhanced inflammation and medial smooth muscle cell proliferation. The resultant neointimal hyperplasia causes restenosis in various pathological conditions.[1]

Bone marrow (BM)-derived endothelial progenitor cells (EPCs) have been isolated from the mononuclear cell (MNC) population in peripheral blood (PB).[2,3] They have differentiated into ECs,[2] suggesting that they may have a potential to accelerate reendothelialization. Recently, transplantation of autologous PB EPCs to balloon-denuded arteries was reported to facilitate reendothelialization of the injured artery.[4,5] Intravenous transfusion of spleen-derived EPCs or EPCs overexpressing eNOS reduces neointimal formation after vascular injury.[6,7] Delivery of primary cultured PB MNCs to balloon-injured arteries leads to accelerated reendothelialization to promote endothelium-dependent vasoreactivity.[8]

Erythropoietin (Epo) stimulates the proliferation and differentiation of erythroid lineage progenitors. Mature ECs express Epo receptors (EpoRs),[9] and Epo induces proangiogenic response in cultivated mature ECs, as evidenced by EC proliferation and migration[10] and the antiapoptotic effect on ECs[11] as well as NO production.[12] Epo increases circulating EPCs to stimulate neovascularization in vivo[13] or induces proangiogenic phenotype in cultured ECs[14] and also improves wound healing by angiogenesis in the genetically diabetic mouse.[15] This evidence leads to the hypothesis that Epo may provide an effective noninvasive strategy to enhance reendothelialization of injured vessels.

Several studies have shown that the exogenous administration of cytokines increases the number of circulating EPCs. For example, pretreatment with vascular endothelial growth factor (VEGF) was reported to double the number of circulating EPCs in humans,[16,17] and the administration of granulocyte colony–stimulating factor (G-CSF) recruited EPCs from BM.[17] Mobilization of the circulating EPCs by exogenous G-CSF facilitates reendothelialization and inhibits neointimal development.[18]

In this study, we evaluated the efficacy of short-term Epo treatment as a strategy for promoting reendothelialization followed by the inhibition of neointimal hyperplasia in

Original received November 28, 2005; revision received March 22, 2006; accepted April 18, 2006.

From the Departments of Cardiovascular Medicine (N.U., M.O., H.Y., A.M., S.M., K.T., T.N., T. Takahashi, T. Tatsumi, H.M.) and Pharmacology (K.M.), Kyoto Prefectural University of Medicine; and Department of Pathology (Y.A.), Kansai Medical University, Osaka, Japan.

Correspondence to Mitsuhiko Okigaki, MD, Department of Cardiovascular Medicine, Kyoto Prefectural University of Medicine, Kamigyo-ku, Kyoto 602-8566, Japan. E-mail okigakim@koto.kpu-m.ac.jp

Circulation Research is available at http://circres.ahajournals.org

DOI: 10.1161/01.RES.0000224117.59417.f3